Integrative Analysis of Differential Gene Expression, Transcript Usage, and RNA Secondary Structure in Early- and Late-Onset Colorectal Cancer

Salomon Elieser Marquez Villalobos

M0.207 Omics Data Analysis

Master in Bioinformatics and Bioestadistics

Name of the tutor:
**Fernando Pastor Rodriguez and Igor Rui
Aliaga**

Name of the SRP:
Diego Garrido Martin

January 4, 2026

Universitat Oberta
de Catalunya

Final Work Card

Title of the work:	Integrative Analysis of Differential Gene Expression, Transcript Usage, and RNA Secondary Structure in Early- and Late-Onset Colorectal Cancer
Name of the author:	Salomon Elieser Marquez Villalobos
Name of the tutor:	Fernando Pastor Rodriguez and Igor Ruiz de los Mozos Aliaga
Name of the SRP:	Diego Garrido Martin
Date of delivery:	January 4, 2026
Studies or Prgram:	Master in Bioinformatics and Bioestadistics
Area or the Final Work:	M0.207 Omics Data Analysis
Language of the work:	English
Keywords:	CRC, DGE, DTU, 2D RNA structure prediction

Abstract

Colorectal cancer is increasingly diagnosed in individuals younger than 50 years, a trend referred to as early-onset colorectal cancer. This study applied an integrative transcriptomic workflow to characterize molecular differences between early-onset and late-onset colorectal cancer. A total of 86 matched tumor and normal samples were analyzed using a combination of differential gene expression, differential transcript usage, and RNA secondary structure prediction.

Differential gene expression analysis identified a 40-gene signature uniquely deregulated in early-onset colorectal cancer, enriched in immune-related, inflammatory, and cell-matrix adhesion processes. Differential transcript usage analysis revealed substantial differences in transcript-level complexity between cohorts, with late-onset colorectal cancer showing extensive isoform remodeling, whereas early-onset tumors displayed a more restricted pattern of transcript usage. Despite these global differences, six conserved isoform switches were consistently detected in both cohorts, including TPM2, LMNB2, MAP3K20, and the long non-coding RNA HOXB-AS3. RNA secondary structure prediction further characterized significant isoforms, revealing a predominance of stem motifs.

These results indicate that gene-level and isoform-level analyses capture complementary aspects of colorectal cancer transcriptomic variation. The integrative framework presented here provides a methodological basis for future large-scale studies and supports the exploration of RNA structural features as potential biomarkers and therapeutic targets in colorectal cancer.

Acknowledgements

To my wife, Angeles, for her unconditional support and affection, and for introducing me to the world of biology and gene therapy.

To my father, Felix and Martina, for their hospitality and care during the writing of this manuscript.

To my supervisors. Fernando, thank you for welcoming me into your laboratory and for providing all the resources necessary to complete this project. Igor, thank you for your experience and guidance, for being a facilitator who shared his passion for teaching.

To my tutor, Diego, for his observations during the execution of this work.

Contents

List of Figures

List of Tables

Chapter 1

Introduction

Colorectal cancer (CRC) is one of the leading causes of cancer-related morbidity and mortality worldwide [1]. Traditionally regarded as a disease predominantly affecting older individuals, recent years have seen a marked increase in cases diagnosed in patients under 50 years of age [2]. This trend, referred to as early-onset colorectal cancer (EOCRC), is associated with distinct clinical, molecular, and prognostic characteristics. Compared with late-onset colorectal cancer (LOCRC), EOCRC tumors more frequently exhibit signet ring cell features [3], tend to arise in the distal colon or rectum [4], and display distinct mutational landscapes, including a lower prevalence of APC-mutated tumors [5]. Elucidating the molecular mechanisms that differentiate EOCRC from LOCRC is therefore critical for improving early detection strategies and guiding more effective therapeutic approaches.

Transcriptome profiling in CRC

Transcriptome analysis using RNA sequencing (RNA-seq) has become a cornerstone in the molecular investigation of colorectal cancer, enabling the identification of genes that are differentially expressed between pathological conditions and healthy controls. This approach has substantially contributed to the discovery of dysregulated pathways and candidate biomarkers associated with colorectal carcinogenesis. A number of studies have reported genes whose expression appears to be associated with EOCRC, including ALDH1A1 [6], PEG10 [7], and ANPEP [8]. Although differences in mutational landscapes between early-onset and late-onset colorectal cancer have been investigated in previous studies [9], comparative analyses of their transcriptional profiles remain relatively limited and have only gained attention in recent years.

Isoform diversity and alternative splicing in CRC

Gene-level differential expression analyses (DGE) provide only a partial representation of the transcriptomic complexity, as a single gene can give rise to multiple transcript isoforms with distinct regulatory and functional properties. Biologically meaningful alterations may occur at the transcript level without being reflected in changes in total gene expression. In this regard, most existing transcriptomic studies of EOCRC [10] have focused primarily on gene-level expression changes, thereby overlooking post-transcriptional regulatory mechanisms that can contribute significantly to transcriptome complexity.

Alternative splicing is a central mechanism of post-transcriptional regulation that increases proteomic diversity by generating multiple mRNA isoforms from the same gene. Importantly, alternative splicing is a major driver of functional diversity in colorectal cancer [11] and is known to be influenced by age, environmental factors [12], and the intestinal microbiome [13]. Aberrant splicing patterns have been widely implicated in the initiation and progression of colorectal cancer and other solid tumors. Despite its biological relevance, isoform-level regulation has not been extensively characterized in EOCRC.

Differential transcript usage (DTU) analysis allows for the detection of changes in the relative proportions of isoforms between conditions independently of gene-level expression differences, offering isoform-specific resolution. Tools such as `IsoformSwitchAnalyzeR` [14] enable the systematic characterization of changes in exon usage, untranslated regions, intron retention, and open reading frames, thereby linking transcript-level variation to potential functional outcomes. Consequently, integrating DGE and DTU analyses can provide a mechanistic framework to interpret how changes in isoform usage may lead to functional divergence beyond expression levels alone in CRC. Addressing this task requires bioinformatics approaches capable of resolving transcript-level variation and integrating it with downstream functional analyses.

RNA structure as a functional layer of transcriptomic regulation in CRC

The function of RNA is not determined solely by its nucleotide sequence or expression level, it is also shaped by the conformations it adopts. RNA molecules can adopt a wide range of structures that are essential for their biological roles [15], such as tRNAs, small nucleolar RNAs, ribosomal RNAs and riboswitches, yet the principles governing RNA folding and the functional relevance of many structural elements remain incompletely understood. As a result, studying the dynamics and functional impact of RNA structure has emerged as a central area of investigation in modern molecular biology.

A practical way to explore how RNA molecules may adopt specific conformations is through computational structure prediction, particularly in cases where experimental determination of RNA structure is not feasible. These approaches are generally most reliable for shorter transcripts, while prediction complexity and uncertainty increase substantially with RNA length. A wide range of algorithms has been developed to infer RNA secondary structures using thermodynamic principles [16, 17], comparative approaches that exploit sequence covariation [18, 19, 20], and machine learning and artificial intelligence–based strategies [21]. Furthermore, motivated by the success of large language models (LLMs) in proteins and DNA [22], a number of RNA-focused LLMs have recently been developed [23] being RNA secondary structure prediction one of their most relevant and impactful applications.

Considering the clinical and molecular differences between younger and older patients with CRC, it is of particular interest to investigate whether age-associated changes in isoform usage translate into alterations in RNA structure. Identifying differentially used transcripts between age groups and analyzing their secondary structures could reveal regulatory mechanisms specific to EOCRC or LOCRC patients.

1.1 Work objectives

1.1.1 General objective

The primary goal of this project is to identify genes and transcripts that are differentially regulated in early-onset and late-onset colorectal cancer, and to evaluate whether changes in isoform usage are associated with differences in their RNA secondary structure through computational prediction.

1.1.2 Specific objectives

- Identify genes differentially expressed between EOCRC and LOCRC samples and characterize the biological pathways associated with transcriptional changes.
- Detect and characterize transcripts exhibiting significant differential usage between EOCRC and LOCRC samples, with emphasis on isoform switching events and alternative splicing.
- Evaluate whether age-associated isoform switches in CRC are associated with changes in predicted RNA secondary structure.

1.2 Focus and method followed

In this work, we adopted an integrative transcriptomic strategy to investigate molecular differences between early-onset and late-onset colorectal cancer (EOCRC and LOCRC). Building upon a previously conducted gene-level study [2], we extend the analysis by incorporating isoform-level regulation and RNA secondary structure prediction, thereby moving beyond expression changes alone to explore post-transcriptional and structural layers of regulation.

Publicly available RNA-seq datasets comprising paired tumor and adjacent normal tissues from EOCRC and LOCRC patients were analyzed to characterize transcriptional regulation at both the gene and isoform levels. Gene-level differential expression analysis (DGE) was performed to establish a baseline view of age-associated transcriptional differences and to identify dysregulated biological pathways. Building on this framework, differential transcript usage (DTU) analyses were conducted to detect changes in isoform proportions, with particular emphasis on alternative splicing and isoform switching events that are not captured by gene-centric approaches.

To investigate the potential functional consequences of age-associated isoform regulation, transcripts exhibiting significant differential usage were further analyzed using computational RNA secondary structure prediction. Predicted structures were assessed both qualitatively and quantitatively to identify structural motifs and features that may differ between age groups, using RNAstructure and the *bpRNA* toolkit. By integrating gene-level expression, isoform-level regulation, and RNA structural analysis, this study aims to provide a multi-layered view of transcriptomic complexity in colorectal cancer and to assess whether age-dependent isoform usage is associated with structural features of potential functional relevance.

1.3 Working Plan

The main milestones for this project are outlined below. Progress was tracked in real time using a dedicated master-bioinformatics GitHub project, which facilitated version control, documentation of analytical decisions, and reproducibility of results.

- M1 (by October 31): RNA-seq processing pipeline deployed and validated on the UNAV HPC cluster, with gene- and transcript-level quantification completed for EOCRC and LOCRC cohorts.
- M2 (by November 30): Differential gene expression and differential transcript usage analyses finalized, including functional and splicing consequence annotation of significant isoform switches.
- M3 (by December 15): RNA secondary structure prediction and structural motif analysis of age-associated isoform switches completed.
- M4 (by December 31): Final manuscript submitted to advisors.

1.3.1 Retrospective risk analysis

Table 1.1 summarizes the main technical and methodological challenges encountered during the development of this project and the mitigation strategies adopted. Detailed progress reports, intermediate analyses, and implementation decisions are available in the master-bioinformatics GitHub repository, ensuring full reproducibility and transparency of the workflow.

1.4 Brief summary of products obtained

This project produced the following deliverables.

- A master's thesis manuscript documenting the analytical workflow, results, and their biological interpretation.
- A configured and validated `nf-core/rnaseq` Nextflow pipeline for reproducible RNA-seq analysis on high-performance computing (HPC) clusters.
- A Zenodo repository https://doi.org/10.5281/zenodo.17801437 hosting primary and processed data generated in this study (access provided upon request).
- A GitHub repository containing primary scripts and documentation (access provided upon request).

Table 1.1: Retrospective analysis of major challenges to implement the project, their impact, and mitigation strategies adopted.

Challenge	Impact on project	Mitigation strategy and outcome
Infrastructure limitations	The original plan to use the RiNALMo language model for RNA secondary structure prediction was not feasible due to GPU architecture incompatibility and memory constraints on the local cluster. RiNALMo requires at least a GPU with 24 GB of memory and a more recent GPU architecture such as L4, A10, or A100.	We applied for external infrastructure access via the EuroCC Spain Testbed program. To ensure timely completion, the project pivoted to RNAstructure, a validated thermodynamics-based structure prediction tool.
Biological complexity and candidate relevance	RNA structure predictions alone risked limited interpretability if applied to weak or biologically irrelevant candidates.	A transcriptomic framework was incorporated to guide candidate selection. Differential gene expression (DGE) and differential transcript usage (DTU) analyses across two datasets with a total of 86 CRC patients ensured that structural analyses targeted high-confidence, age-associated isoform switches.

1.5 Brief description of other memory chapters

The following chapters present a structured overview of the work carried out in this study. Chapter 2 details the materials, datasets, and computational methods employed, including data acquisition, transcriptomic analyses, and RNA structure prediction workflows. Chapter 3 reports the main results derived from these analyses, covering gene- and isoform-level findings as well as structural insights. Chapter 4 discusses these results in the context of existing literature, highlighting their biological relevance and methodological implications. Finally, Chapter 5 summarizes the main conclusions of the study and outlines potential directions for future research building on the findings presented here.

Chapter 2

Materials and methods

In this section, we describe the datasets, computational tools, and analytical workflows implemented to investigate transcriptomic differences between EOCRC and LOCRC cohorts. The overall integrative analysis workflow is summarized in Figure 2.1.

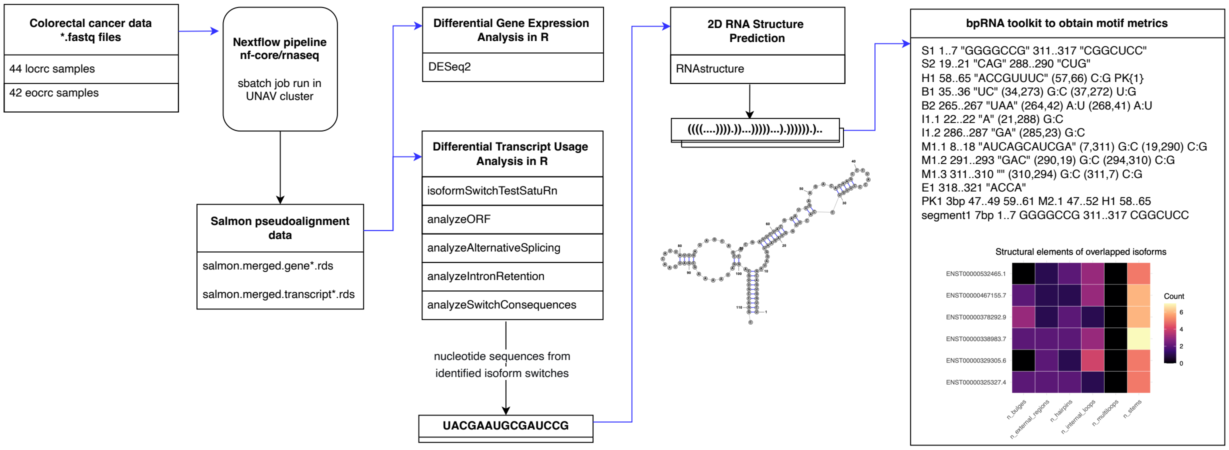

```
S1 1..7 "GGGGCCG" 311..317 "CGGCUCC"
S2 19..21 "CAG" 288..290 "CUG"
H1 58..65 "ACCGUUUC" (57,66) C:G PK{1}
B1 35..36 "UC" (34,273) G:C (37,272) U:G
B2 265..267 "UAA" (264,42) A:U (268,41) A:U
I1.1 22..22 "A" (21,288) G:C
I1.2 286..287 "GA" (285,23) G:C
M1.1 8..18 "AUCAGCAUCGA" (7,311) G:C (19,290) C:G
M1.2 291..293 "GAC" (290,19) G:C (294,310) C:G
M1.3 311..310 "" (310,294) G:C (311,7) C:G
E1 318..321 "ACCA"
PK1 3bp 47..49 59..61 M2.1 47..52 H1 58..65
segment1 7bp 1..7 GGGGCCG 311..317 CGGCUCC
```

Figure 2.1: Schematic overview of the integrative transcriptomic analysis workflow implemented in this study.

2.1 Data acquisition

The RNA-seq data used in this work were obtained from the NCBI Gene Expression Omnibus (GEO) database. The SRA study SRP357925 dataset comprises 21 pairs of EOCRC patients and the SRA study SRP479528 dataset 22 pairs of LOCRC patient. The pairs include both tumor tissues and matched adjacent normal tissues from rectum, sigmoid colon, ascending colon, descending colon, and cecum, providing a comprehensive resource for differential expression and transcript usage analyses. The raw sequencing data were downloaded in FASTQ format onto the UNAV cluster using the SRA Toolkit [24].

2.2 RNAseq pipeline implementation

Gene expression quantification was carried out with the `nf-core/rnaseq` workflow [25]. This pipeline, built on Nextflow, provides a standardized and fully reproducible framework for processing raw FASTQ files and obtaining expression estimates because the codebase is versioned and publicly maintained on GitHub.

All samples in this project were analyzed using `nf-core/rnaseq v3.21.0` using the University of Navarra high-performance computing cluster. The specific implementation used for this work is available in the master-bioinformatics GitHub repository. Before quantification, raw reads underwent quality inspection with FastQC, followed by adapter and low-quality base trimming using TrimGalore. Transcript abundance was then estimated with *Salmon* [26], which performed a fast pseudo-alignment procedure rather than a full genomic alignment. Salmon built an index of the transcriptome and mapped sequencing fragments to it, enabling efficient inference of transcript-level expression. To build the Salmon index, we used the `GRCh38.primary_assembly.genome.fa.gz` file as the reference genome and the `gencode.v49.primary_assembly.annotation.gtf.gz` as the gene annotation file.

2.3 Differential expression analysis

We used *DESeq2* [27] to identify statistically significant differences in expression levels between conditions. We removed genes with less than 10 counts on all samples. This practice saved us computational resources when conducting the DGE analysis. To account for differences in library size and composition differences before downstream analyses, we performed normalization by sequencing depth of raw counts. The size factor was calculated using the $estimateSizeFactor()$ function. Next, normalization of samples was performed through the variance stabilizing transformation (vst) function of the *DESeq2* package. Principal component analysis was run with the *prcomp* command. Heatmaps were created using the *pheatmap* function in R using unsupervised hierarchical clustering and scaling by row unless otherwise noted.

Following differential expression analysis with *DESeq2*, we performed gene set enrichment analysis (GSEA) to investigate enriched biological pathways and processes. GSEA accounts for expression levels across all genes detected in a sample. This analysis was carried out using the *clusterProfiler* R package [28].

2.4 Differential transcript usage analysis

Differential transcript usage (DTU) analysis was performed on the University of Navarra HPC cluster using the *IsoformSwitchAnalyzeR* [14] library. Code details are available in the master-bioinformatics GitHub repository.

Salmon quantification files (`quant.sf`) obtained from the `nf-core/rnaseqpipeline`, corresponding to 42 EOCRC and 44 LOCRC samples, were imported using the `importIsoformExpression` and `importRdata` functions to create a `switchAnalyzeRlist` object. The GENCODE v49 reference transcript sequences `gencode.v49.transcripts.fa.gz` and corresponding annotation gencode.v49.primary_assembly.annotation.gtf.gz were supplied to the isoformNtFasta and isoformExonAnnotation parameters, respectively.

Data were filtered using a gene expression cutoff=1; isoform expression cutoff=0, which completely removed unused isoforms; IFcutoff=0, which removed non-contributing isoforms and removed single isoform genes. Although DEXSeq is commonly recommended for differential isoform usage testing, it is computationally inefficient for *large datasets* [29]. Therefore, we used the isoformSwitchTestSatuRn function to test for differential transcript usage.

2.5 Splicing analysis

Open reading frames were predicted using analyzeORF to assess coding potential. Alternative splicing patterns were characterized with analyzeAlternativeSplicing, and intron retention events were identified using analyzeIntronRetention. Finally, the functional impact of isoform switches was evaluated with analyzeSwitchConsequences, integrating changes in coding capacity and splicing features to infer potential biological effects. Finally, we used extractSplicingSummary and extractConsequenceSummary functions to quantify gain/loss of predicted splicing events such as exon skipping and intron retention.

2.6 RNA secondary structure prediction

The secondary structures of the top isoforms exhibiting differential transcript usage (DTU) in both EOCRC and LOCRC samples were predicted using the *RNAStructure* software [16]. Isoform sequences were retrieved from the IsoformSwitchAnalyzeR object via the extractSequence function. *RNAStructure* was run locally on a macOS system equipped with 16GB RAM and 2,5 GHz Dual-Core Intel Core i7. Predicted structures were visualized using the *RNAStructure* graphical user interface (GUI) to identify conserved motifs and structural features of potential functional relevance.

For quantitative motif analysis including hairpin, loops, bulges, and internal loops, we employed the *bpRNA* toolkit [30]. The secondary structures predicted by *RNAStructure* were submitted to *bpRNA*, which generated detailed annotations of structural motifs and their properties. This approach enabled the systematic identification of potential functional RNA elements that may contribute to the biological mechanisms underlying colorectal cancer.

2.7 Data availability

Datasets generated and analyzed during this study are available in the Zenodo repository under accession DOI: 10.5281/zenodo.17801437.

Chapter 3

Results

In this section we present the main findings from the integrative transcriptomic analysis of early-onset and late-onset colorectal cancer.

3.1 Nextflow nf-core/rnaseq pipeline implementation and validation

The `nf-core/RNAseq` pipeline was successfully deployed on the University of Navarra HPC cluster to process 86 samples from EOCRC and LOCRC cohorts. The pipeline was configured to use *Salmon* for transcript quantification, leveraging its fast pseudo-alignment capabilities to efficiently estimate transcript abundances. The EOCRC workflow took 2.5h and 192.2 cpu-hours while the LOCRC workflow took 1.5h and 188.4 cpu-hours to complete.

Nextflow execution reports and MultiQC summaries are available in the directories `reports_sra_srp357925_gencode_samples_42` and `reports_sra_srp479528_gencode_samples_44` within the master-bioinformatics GitHub project. Processed RNA sequencing samples generated using *Salmon* pseudoalignment are available via Zenodo under the files `rnaseq_salmon_results_gencode_samples_42.tar.gz` and `rnaseq_salmon_results_gencode_samples_44.tar.gz`.

3.2 PCA and sample clustering analysis

Exploratory transcriptome analysis was performed for both EOCRC and LOCRC cohorts to assess sample structure and global expression patterns. Normalization and transformation of expression counts resulted in stabilized distributions across samples, supporting their use for downstream multivariate analyses, see Appendix A and Appendix B.

Principal component analysis revealed a clear separation between normal and tumor tissues in the LOCRC cohort, whereas EOCRC samples did not show a distinct segregation by tissue type, see Figure 3.1 and Figure 3.2. Instead, EOCRC samples exhibited a more heterogeneous structure, with k-means clustering suggesting partitioning into three groups, independent of tissue status.

In both cohorts, the first two principal components captured a comparable proportion of variance, with PC1 and PC2 explaining approximately 26% of the total variability in EOCRC and 27.4% in LOCRC. Distance-based analyses were consistent with the PCA results, as sample-to-sample distance heatmaps and hierarchical clustering supported the observed cohort-specific structure and did not indicate the presence of strong technical artifacts, see Figure A.4 and Figure B.4.

Outlier detection based on Mahalanobis distance identified one potential outlier in each cohort, namely sample srr17866844 in EOCRC and srr27320659 in LOCRC, both derived from normal tissue. These samples were retained in the analysis, as their matched tumor counterparts did not display outlier behavior.

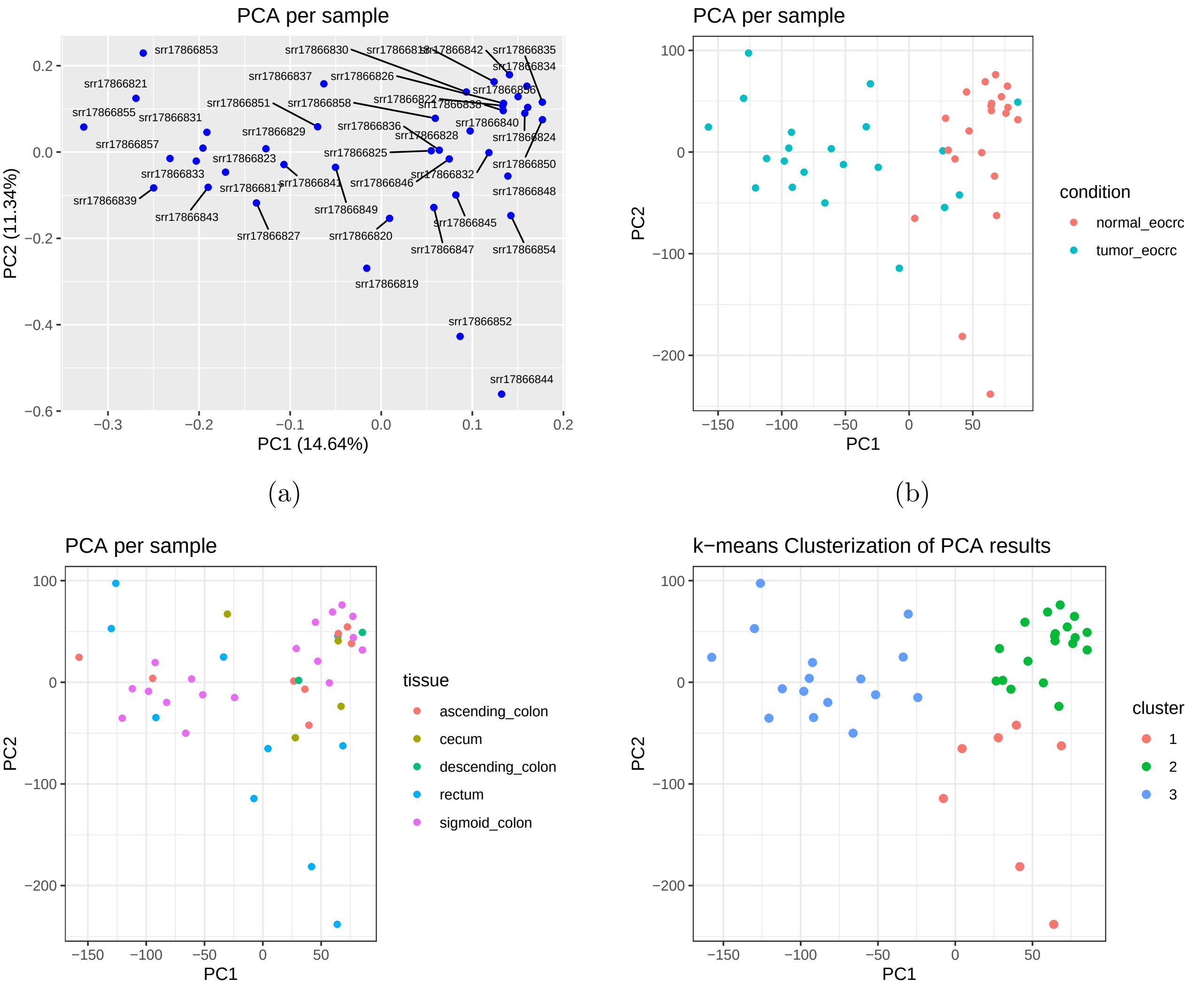

(a)

(b)

(c)

(d)

Figure 3.1: EOCRC samples showing variance stabilizing transformation (vst) normalized counts. (a) PCA plot colored by sample. (b) PCA plot colored by condition tumor vs normal. (c) PCA plot colored by tissue type. (d) PCA plot colored by clusterization.

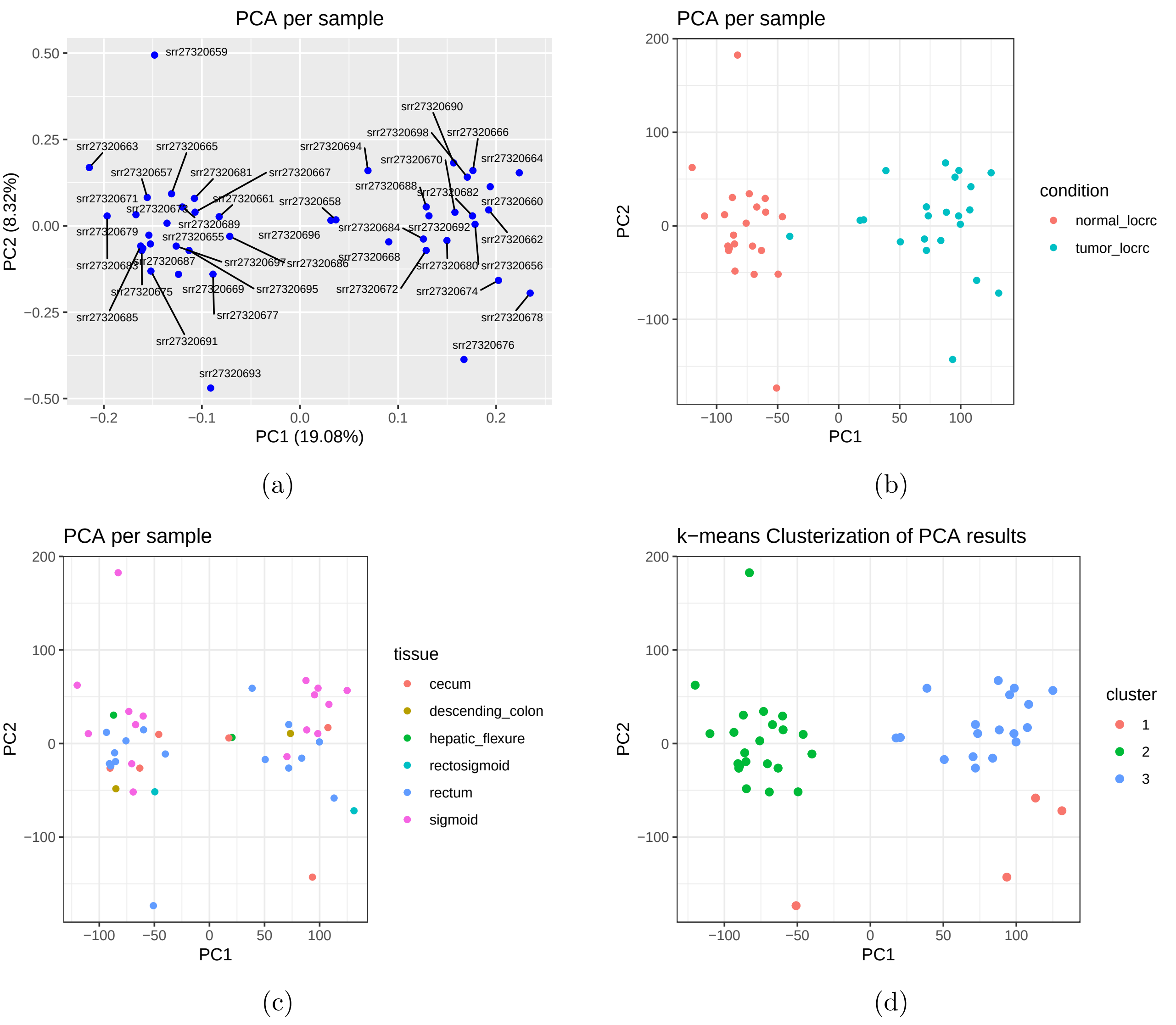

(a)

(b)

(c)

(d)

Figure 3.2: LOCRC samples showing variance stabilizing transformation (vst) normalized counts. (a) PCA plot colored by sample. (b) PCA plot colored by condition tumor vs normal. (c) PCA plot colored by tissue type. (d) PCA plot colored by clusterization.

3.3 Identification of differentially expressed gene signatures

Volcano plots in Figure 3.3 display the distribution of differentially expressed genes (DEGs) in EOCRC and LOCRC samples using *DESeq2*. For more details about the DGE analysis, check the *Rmd* scripts at master-bioinformatics GitHub project. Top DEGs of each cohort ordered by *padj* are summarized in Table A.1 and Table B.1, respectively.

Genes were classified as non-significant in LOCRC when the `adjusted p-value > 0.2`, the `|LFC|` $<$ 0.7, and the `meanBase > 50` counts, defining a background set for comparison. In contrast, EOCRC-specific differential expression was defined using stricter criteria. Upregulated genes required an `adjusted p-value < 0.05`, the `LFC > 1`, and the `meanBase > 50`,

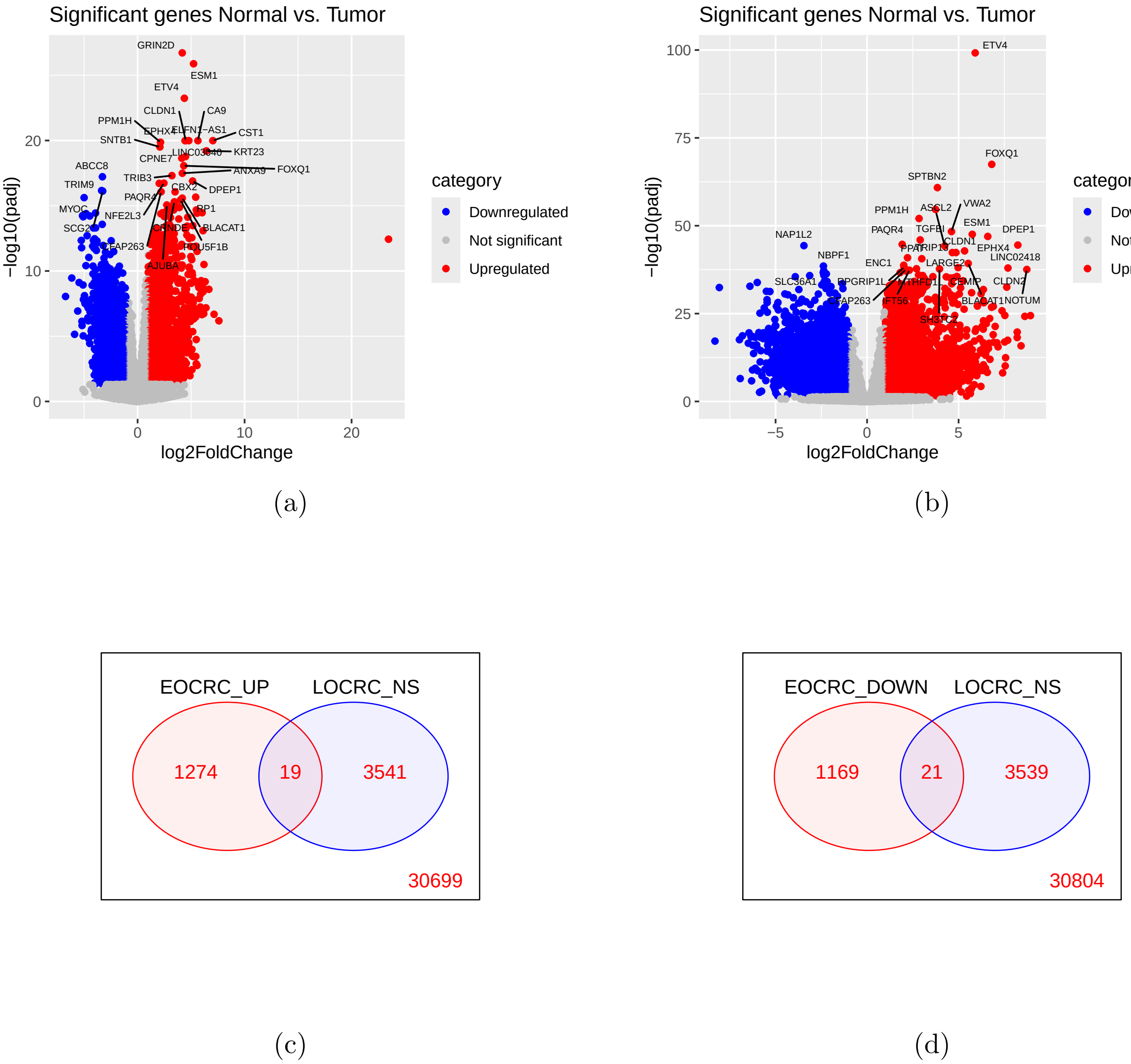

(a)

(b)

(c)

(d)

Figure 3.3: Volcano plots of differentially expressed genes (DEGs). Red dots indicate significantly upregulated (right) and downregulated (left) genes `|logFC| > 1, p < 0.05`. (a) EOCRC samples. (b) LOCRC samples. Venn diagrams show the overlap of DEGs between EOCRC and LOCRC for (c) upregulated and (d) downregulated genes.

while downregulated genes required an `adjusted p-value < 0.05`, the `LFC < -1`, and the `meanBase > 50`. Venn diagrams summarizing these results identified distinct sets of genes uniquely dysregulated in EOCRC relative to LOCRC.

A total of 40 genes were identified as specific to EOCRC, comprising 19 upregulated and 21 downregulated genes that were significantly deregulated in younger patients but not in individuals with later-onset disease, check Table 3.1. Comparison with the reference study [2] revealed that 30 of these genes overlapped with their reported list of 48 genes. The overlapping genes were ARHGAP6, WNT11, MSLN, TFPI2, NPTX2, NRXN2, CCR7, HSPA2, STEAP4, HOXD9, IL1RN, DUOX2, TRIM7, STC1, SLC38A11, FIBIN, TMEM45A, PRKD1, IFITM2, C16orf54, L1CAM, IGLV5-45, IGHV1-3, IGHV3-13, IGHV4-39, MEG3, IGHV3-74, IGKV1-12,

Table 3.1: Top DEGs between EOCRC and LOCRC samples. Significance cutoffs were as follows: LOCRC: adjusted p-value > 0.2, LFC < 0.7, mean counts>50; EOCRC Up: adjusted p-value < 0.05, LFC > 1, mean counts > 50; EOCRC Down: adjusted p-value < 0.05, LFC < -1, mean counts>50.

Gene	EOCRC_baseMean	EOCRC_log2FC	EOCRC_padj	LOCRC_baseMean	LOCRC_log2FC	LOCRC_padj	Direction
WNT11	182.214	1.820	0.001	111.907	0.544	0.257	Up
SCD	4216.099	1.099	0.025	6498.227	0.657	0.238	Up
MSLN	760.166	2.326	0.000	287.297	0.497	0.309	Up
TFPI2	73.805	1.257	0.023	211.037	0.668	0.382	Up
NAMPT	4747.169	1.012	0.001	6665.529	0.378	0.293	Up
NPTX2	288.510	2.551	0.000	59.192	0.592	0.347	Up
IL1RN	572.677	1.336	0.017	273.531	0.480	0.239	Up
DUOX2	3200.761	1.513	0.002	3291.115	0.390	0.475	Up
TRIM7	102.093	1.395	0.010	53.860	0.157	0.809	Up
FCGR1A	132.163	1.348	0.004	76.052	0.338	0.456	Up
STC1	180.853	1.735	0.001	168.280	0.543	0.332	Up
METTL27	168.208	1.117	0.022	65.197	0.319	0.493	Up
NA	257.201	1.005	0.013	141.321	0.345	0.466	Up
FIBIN	89.580	1.067	0.012	109.365	0.520	0.276	Up
TMEM45A	175.731	1.181	0.013	101.481	-0.087	0.806	Up
IFITM2	3696.455	1.165	0.005	2285.358	0.435	0.358	Up
EIF3CL	120.863	1.164	0.028	205.005	0.440	0.243	Up
LOC105374041	135.142	1.009	0.030	93.685	0.446	0.383	Up
RNU2-1	356.271	1.648	0.006	69.081	0.225	0.726	Up
ARHGAP6	102.903	-1.172	0.008	125.788	-0.377	0.404	Down
NRXN2	102.621	-1.293	0.008	105.850	-0.176	0.755	Down
CCN2	2246.381	-1.014	0.011	1437.222	-0.396	0.202	Down
CCR7	194.178	-1.046	0.046	60.514	-0.470	0.243	Down
HSPA2	539.285	-1.876	0.000	777.085	-0.376	0.502	Down
STEAP4	158.639	-1.525	0.004	127.669	-0.404	0.388	Down
HOXD9	100.154	-1.214	0.024	69.589	-0.186	0.743	Down
IKZF3	335.876	-1.079	0.018	275.032	-0.475	0.250	Down
SLC38A11	70.097	-1.267	0.001	113.225	0.277	0.591	Down
PRKD1	53.883	-1.003	0.004	58.657	-0.255	0.483	Down
C16orf54	106.184	-1.343	0.000	91.462	-0.181	0.767	Down
L1CAM	119.454	-1.266	0.014	172.464	-0.011	0.990	Down
IGLV5-45	283.873	-1.381	0.018	211.831	-0.515	0.449	Down
IGHV1-3	854.746	-1.328	0.046	454.619	0.102	0.908	Down
IGHV3-13	134.847	-1.554	0.008	181.436	0.368	0.641	Down
IGHV4-39	1823.080	-1.294	0.044	1309.234	-0.073	0.921	Down
MEG3	297.816	-1.160	0.006	242.193	-0.211	0.610	Down
IGHV3-74	1277.028	-1.291	0.027	1199.140	-0.390	0.528	Down
IGKV1-12	1713.942	-1.253	0.014	1392.844	-0.549	0.372	Down
IGHV2-70	181.679	-1.368	0.043	122.798	0.304	0.707	Down
IGHV4-4	667.990	-1.466	0.011	341.672	-0.371	0.558	Down

IGHV2-70, and IGHV4-4. Furthermore, from the curated set of eight genes that they reported, four genes: IL1RN, MSLN, SLC38A11, and WNT11 were also present in the EOCRC-specific gene set identified in our analysis.

To functionally characterize the differentially expressed genes, gene ontology analysis was performed on the 40 genes specific to EOCRC, see Table 3.1. This analysis identified significant enrichment of immune-related biological processes, predominantly associated with adaptive immunity and immunoglobulin-mediated responses, as shown in Figure 3.4.

A gene–concept network was generated to visualize the relationships between enriched GO terms and their associated genes. The network highlights genes shared across multiple immune-related biological processes and illustrates the relative significance of each functional category, see Figure 3.4. These immune-related processes are consisted with those related to humoral and immunoglobulin-mediated immune responses from the reference study [2].

Additional enriched processes were related to inflammatory regulation and immune signaling. Beyond immune-specific categories, enrichment was also observed for adhesion-related processes.

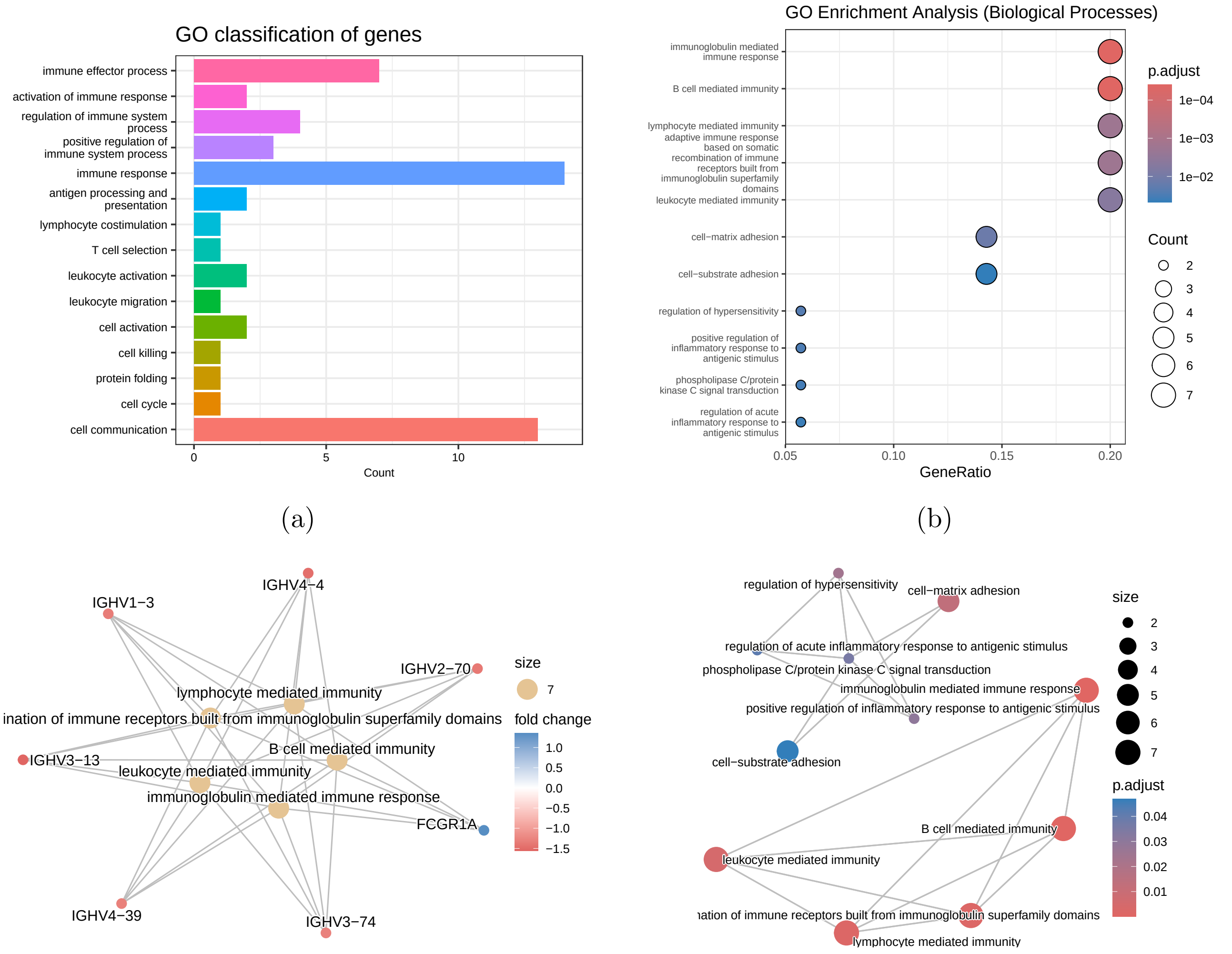

(a)

(b)

(c)

(d)

Figure 3.4: Enrichment analysis of Gene Ontology (GO) terms and pathways for biological processes of genes unique to EOCRC. (a) GO terms enrichment. (b) Pathway enrichment. (c) Gene concept network plot. (d) Enrichment map plot.

3.4 Differential transcript usage analysis

Figure 3.5 illustrates differential transcript usage (DTU) patterns between EOCRC and LOCRC cohorts, analyzed through `IsoformSwitchAnalyzeR` with `isoformSwitchTestSatuRn` as the statistical engine. Transcripts were classified as significantly switched based on isoform fraction change `|dIF|` > 0.05 and `q < 0.05`. For detailed methodology on DTU analysis, refer to the `Rmd` scripts at master-bioinformatics GitHub project.

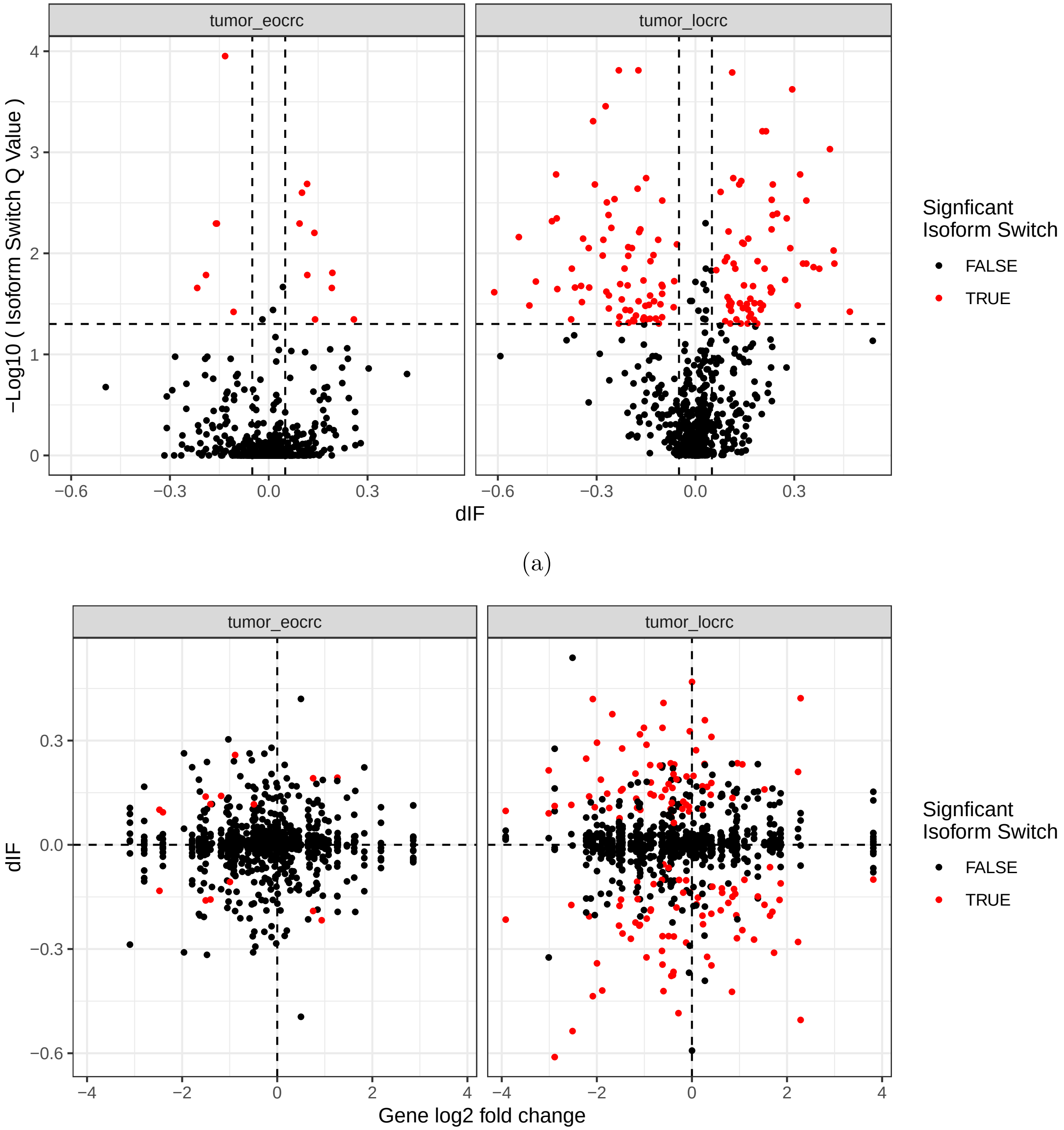

(a)

(b)

Figure 3.5: (a) Isoform switch significance plot of `tumor_eocrc vs_tumor_locrc` highlighting the magnitude and statistical significance of isoform switching events `|dIF| > 0.05, q < 0.05`. (b) Relationship between differential gene expression and isoform switching to assess the independence of isoform switching from overall gene expression changes.

Differential transcript usage analysis was performed to quantify isoform switching events between normal and tumor tissues in EOCRC and LOCRC cohorts as Table 3.2 shows.

Table 3.2: Summary of isoform switching statistics.

Comparison	nrIsoforms	nrSwitches	nrGenes
normal_eocrc vs tumor_eocrc	14	14	10
normal_locrc vs tumor_locrc	140	189	103
Combined	148	198	109

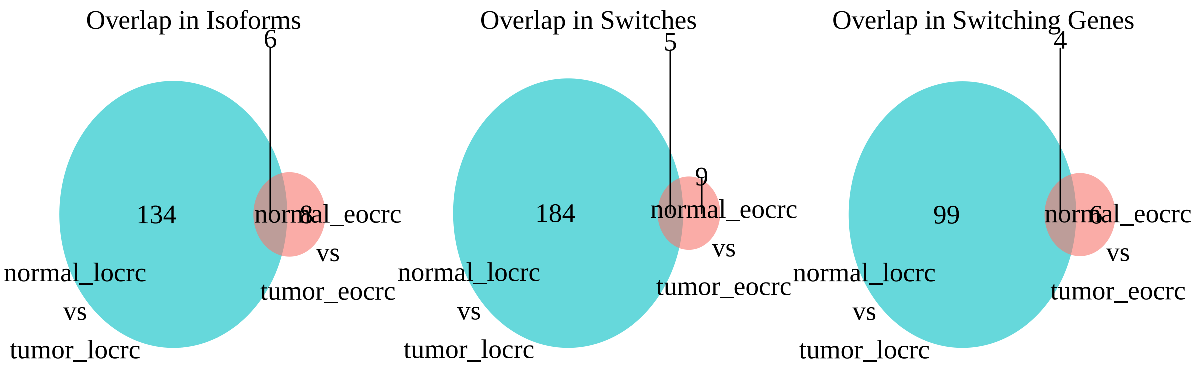

Figure 3.6: Venn diagrams showing the overlap of isoforms and genes with differential transcript usage (DTU) between EOCRC and LOCRC samples.

The EOCRC comparison revealed a limited number of isoform switches, with 14 events affecting 10 genes, indicating minimal transcript-level remodeling. In contrast, the LOCRC comparison showed substantially greater complexity, with 140 isoform switches across 103 genes, including multiple switches per gene (189). Venn diagrams show the overlap of isoforms and genes between EOCRC and LOCRC samples, see Figure 3.6. Table C shows the complete list of 148 isoform switches identified across both cohorts.

3.5 Overlapped isoforms between EOCRC and LOCRC

Table 3.3 summarizes the six isoforms found to be shared between both cohorts corresponding to four genes: TPM2, LMNB2, MAP3K20, and HOXB-AS3. These shared events involved both protein-coding genes and long non-coding RNAs and showed concordant directions of isoform usage change between normal and tumor samples.

Table 3.3: Overlapped isoforms and genes with DTU between EOCRC and LOCRC samples.

isoform_id	gene_name	iso_biotype	condition_1	condition_2	dIF	isoform_switch_q_value	gene_switch_q_value	gene_log2_fold_change	direction
ENST00000378292.9	TPM2	protein_coding	normal_eocrc	tumor_eocrc	-0.1325	1.12e-04	1.12e-04	-2.4767	Down in tumor
ENST00000378292.9	TPM2	protein_coding	normal_locrc	tumor_locrc	-0.1732	1.54e-04	1.54e-04	-2.5368	Down in tumor
ENST00000338983.7	MAP3K20	protein_coding	normal_locrc	tumor_locrc	-0.2728	3.50e-04	3.50e-04	1.3062	Down in tumor
ENST00000329305.6	TPM2	protein_coding	normal_locrc	tumor_locrc	0.1148	0.0018	1.54e-04	-2.5368	Up in tumor
ENST00000329305.6	TPM2	protein_coding	normal_eocrc	tumor_eocrc	0.1009	0.0025	1.12e-04	-2.4767	Up in tumor
ENST00000532465.1	LMNB2	protein_coding_CDS_not_defined	normal_locrc	tumor_locrc	-0.2457	0.0029	0.0029	1.0612	Down in tumor
ENST00000325327.4	LMNB2	protein_coding	normal_locrc	tumor_locrc	0.2315	0.003	0.0029	1.0612	Up in tumor
ENST00000467155.7	HOXB-AS3	lncRNA	normal_locrc	tumor_locrc	-0.1366	0.012	0.012	-0.0406	Down in tumor
ENST00000532465.1	LMNB2	protein_coding_CDS_not_defined	normal_eocrc	tumor_eocrc	-0.1905	0.0164	0.0164	0.755	Down in tumor
ENST00000325327.4	LMNB2	protein_coding	normal_eocrc	tumor_eocrc	0.1915	0.022	0.0164	0.755	Up in tumor
ENST00000338983.7	MAP3K20	protein_coding	normal_eocrc	tumor_eocrc	-0.2172	0.022	0.022	0.9346	Down in tumor
ENST00000467155.7	HOXB-AS3	lncRNA	normal_eocrc	tumor_eocrc	-0.1069	0.038	0.038	-0.9954	Down in tumor

The long non-coding RNA HOXB-AS3 isoform ENST00000467155.7 exhibited a significant reduction in isoform usage in tumors in both cohorts, see Figure 3.7. Isoform fraction decreased in EOCRC (dIF $= -0.107$, q $= 0.038$) and in LOCRC (dIF $= -0.137$, q $= 0.012$), accompanied by reduced isoform expression in tumors.

For LMNB2, two isoforms showed reciprocal switching, see Figure 3.8. Isoform ENST00000325327.4 increased in tumors, with isoform fraction rising in EOCRC (dIF $= 0.192$, q $= 0.022$) and in LOCRC (dIF $= 0.232$, q $= 0.003$), becoming the dominant isoform in both cohorts. Conversely, ENST00000532465.1 decreased in usage in both cohorts, indicating redistribution of isoform usage within the gene.

As Figure 3.9 shows, the protein-coding gene MAP3K20 showed a consistent decrease in usage of isoform ENST00000338983.7 in tumors. Isoform fraction declined in EOCRC (dIF $= -0.217$, q $= 0.022$) and in LOCRC (dIF $= -0.273$, q $= 0.00035$).

In TPM2, isoform switching involved coordinated loss and gain of isoform usage, see Figure 3.10. The major isoform ENST00000378292.9 decreased in tumors in both EOCRC (dIF $= -0.133$, q $= 0.00011$) and LOCRC (dIF $= -0.173$, q $= 0.00015$), while the minor isoform ENST00000329305.6 increased in usage in EOCRC (dIF $= 0.101$, q $= 0.0025$) and LOCRC (dIF $= 0.115$, q $= 0.0018$).

Overall, these shared isoform switching events demonstrate reproducible transcript-level alterations across cohorts, with changes primarily reflecting shifts in isoform contribution rather than uniform changes in gene expression.

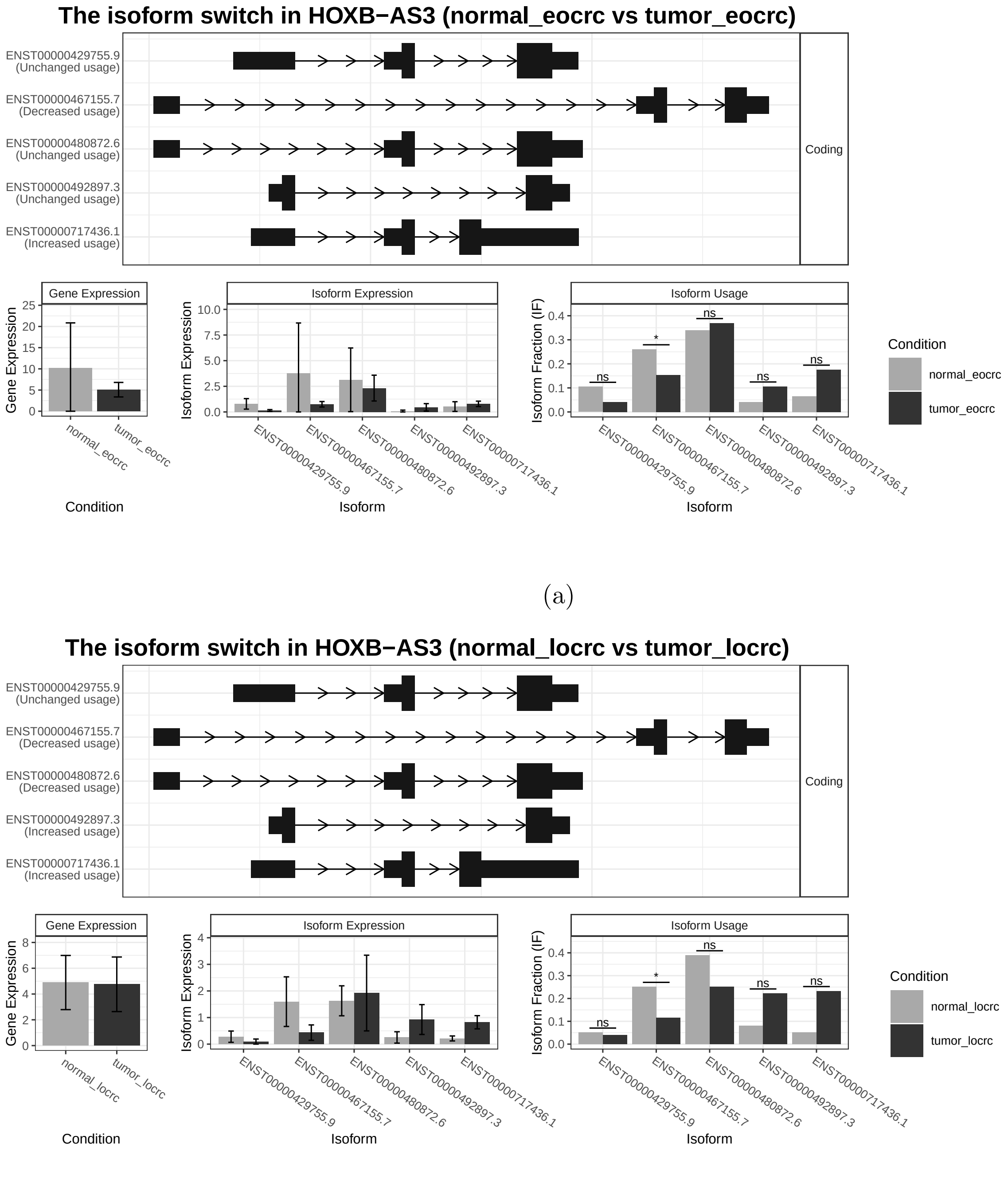

(a)

(b)

Figure 3.7: Isoform switch visualization of the HOXB-AS3 gene highlighting ENST00000467155.7. Panels show differential isoform usage between normal and tumor samples in (a) the EOCRC cohort and (b) the LOCRC cohort, with isoform fraction changes and statistical significance indicated.

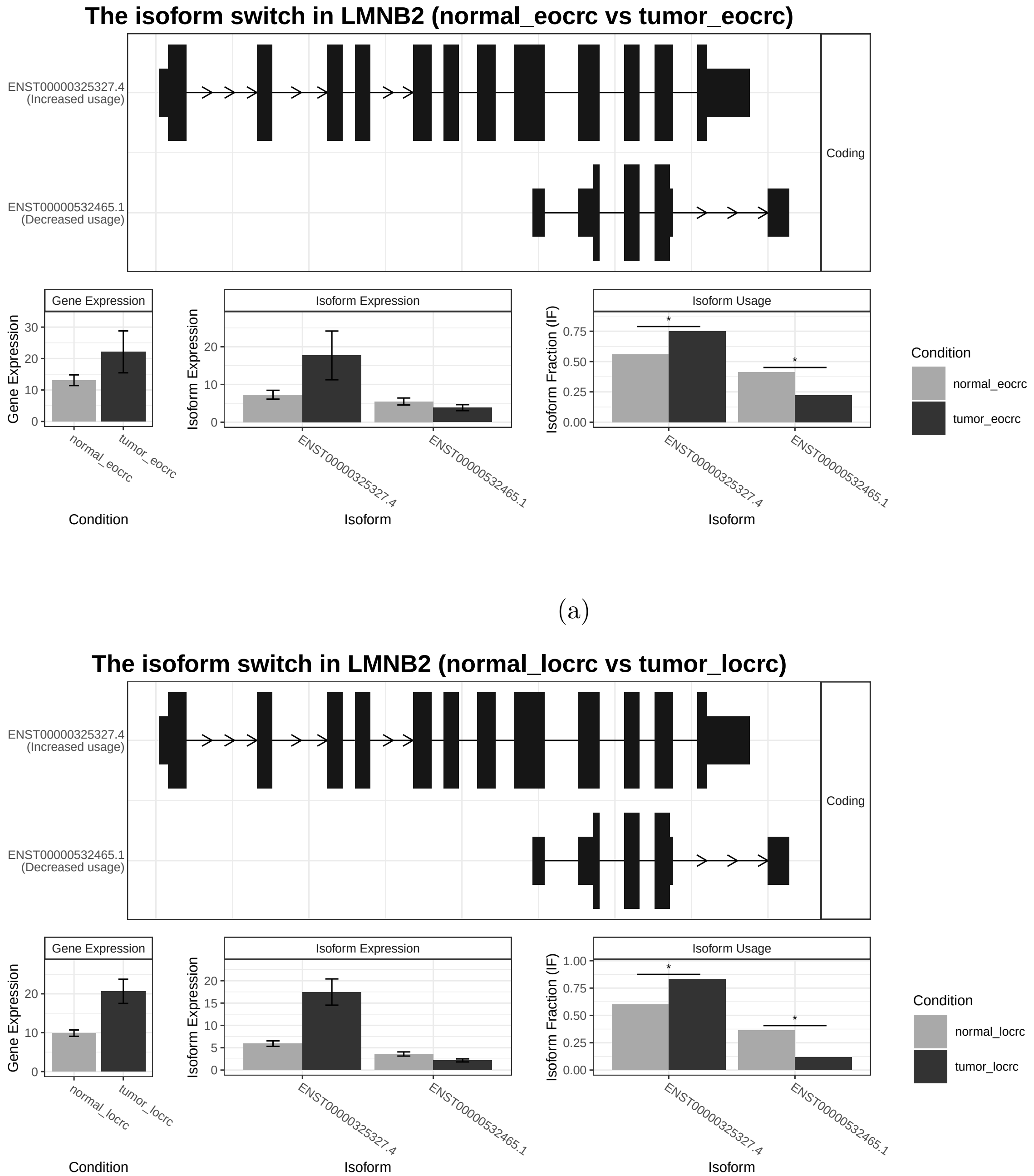

(a)

(b)

Figure 3.8: Isoform switch visualization of the LMNB2 gene highlighting ENST00000325327.4 and ENST00000532465.1. Panels show differential isoform usage between normal and tumor samples in (a) the EOCRC cohort and (b) the LOCRC cohort, with isoform fraction changes and statistical significance indicated.

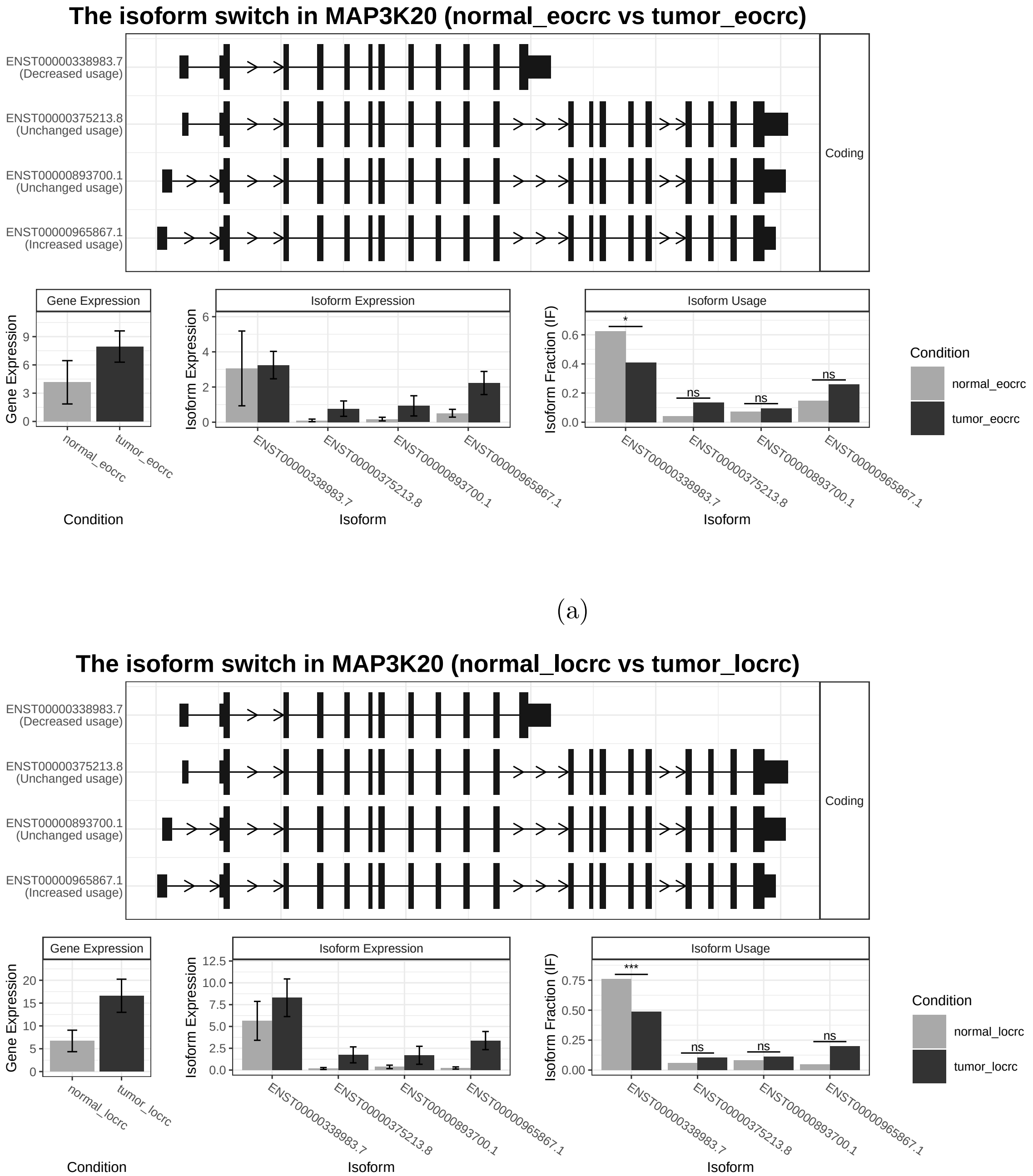

(a)

(b)

Figure 3.9: Isoform switch visualization of the MAP3K20 gene highlighting ENST00000338983.7. Panels show differential isoform usage between normal and tumor samples in (a) the EOCRC cohort and (b) the LOCRC cohort, with isoform fraction changes and statistical significance indicated.

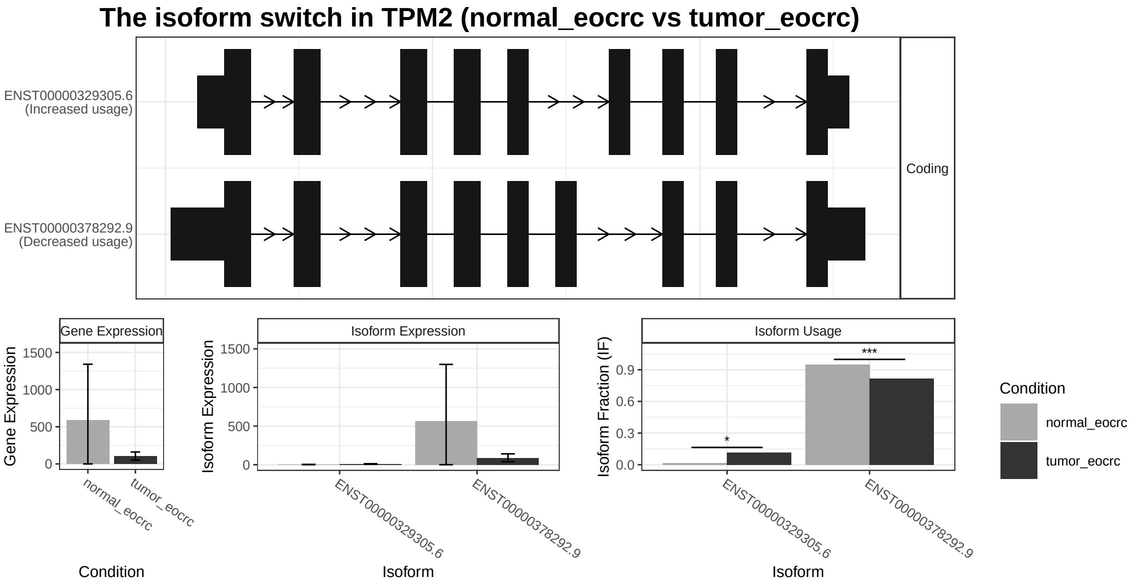

(a)

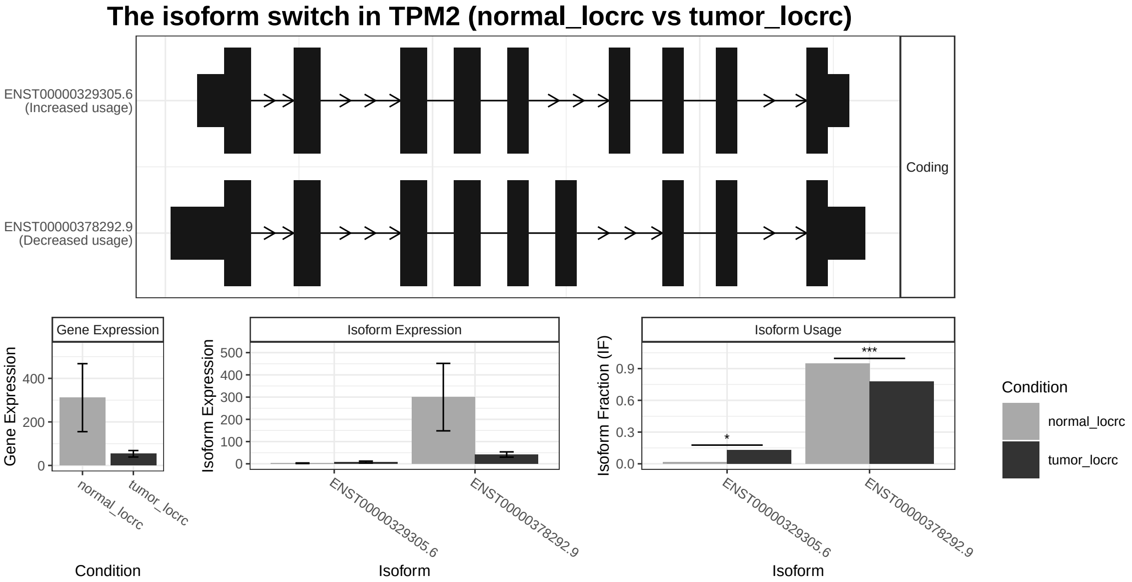

(b)

Figure 3.10: Isoform switch visualization of the TPM2 gene highlighting ENST00000329305.6 and ENST00000378292.9. Panels show differential isoform usage between normal and tumor samples in (a) the EOCRC cohort and (b) the LOCRC cohort, with isoform fraction changes and statistical significance indicated.

3.6 Splicing regulation differences between EOCRC and LOCRC samples

Differential transcript usage analysis revealed that EOCRC tumors exhibit a restricted splicing landscape compared to LOCRC. Alternative 3' splice site events involved 7 isoforms in EOCRC, whereas 95 isoforms were affected in LOCRC. Similarly, alternative 5' splice sites were altered in 9 isoforms in EOCRC and 66 isoforms in LOCRC. Exon skipping events followed the same trend, with 8 isoforms affected in EOCRC versus 115 in LOCRC. Other splicing categories, including alternative transcription start and termination sites, mutually exclusive exons, and intron retention, showed consistently higher isoform counts in LOCRC, see Figure 3.11. These observations indicate that early-onset tumors display subtle transcript-level changes, while late-onset tumors undergo widespread isoform remodeling.

Analysis of the predicted functional consequences of isoform switching supported this pattern. EOCRC tumors displayed a limited number of structural changes at the transcript level, with 3 isoforms gaining exons and 4 losing them. Intron retention was rare, affecting only a single isoform. Shifts in transcription start and termination sites were also modest, with six isoforms starting more downstream and four more upstream, and five isoforms ending more downstream and six more upstream. In contrast, LOCRC tumors showed extensive structural remodeling, including 60 isoforms gaining exons, 37 losing exons, 11 isoforms gaining intron retention, and eight losing it. Start and termination site shifts were widespread, affecting 48 and 64 isoforms for transcription start sites and 34 and 51 isoforms for transcription termination sites in downstream and upstream directions, respectively. No intron structure consequences were predicted in either cohort, see Figure 3.11.

Comparison of structural consequences between cohorts revealed that the relative direction of changes was largely conserved. EOCRC isoforms exhibited slightly more exon losses compared to LOCRC, but this difference was not statistically significant, see Figure 3.12. Similar patterns were observed for intron retention and transcription start and termination site shifts, with Fisher's exact tests confirming no significant differences. These results indicate that while EOCRC and LOCRC differ in the total number of affected isoforms, the balance between gain and loss or upstream and downstream shifts remains consistent across both cohorts.

A genome-wide assessment of isoform usage further confirmed that overall transcript usage is stable. In EOCRC, differences ranged from -0.07 to 0.19, while in LOCRC, differences were generally below 0.10. Statistical testing showed no significant changes, see Figure 3.12.

A direct comparison between the alternative splicing analysis reported by Marx et al. [2] and our isoform switch analysis performed on the same dataset revealed marked differences in the number and nature of detected transcriptomic alterations. Using rMATS and Whippet, Marx et al. identified 82 significantly differentially spliced events in EOCRC tumors compared to normal tissue and 191 events in LOCRC, with 49 events shared between cohorts. In contrast, differential transcript usage analysis using `IsoformSwitchAnalyzeR` condensed these splicing alterations into a smaller set of consequential isoform switches, affecting 10 genes in EOCRC and 103 genes in LOCRC. Among these, four genes exhibited isoform switching in both patient cohorts: TPM2, LMNB2, MAP3K20, and HOXB-AS3.

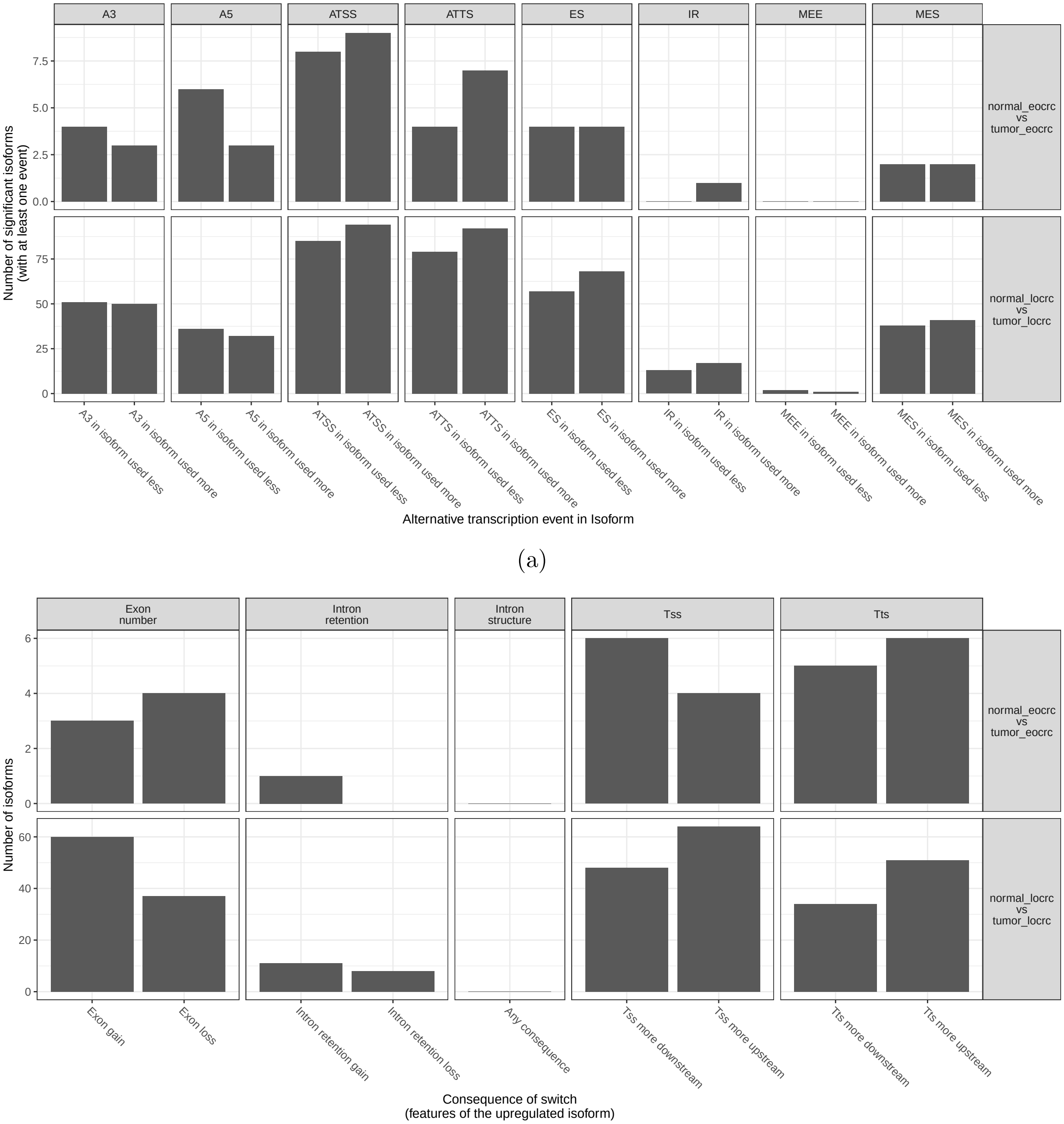

(a)

(b)

Figure 3.11: (a) Summary of alternative splicing event types associated with isoform switches in EOCRC and LOCRC, including alternative splice site usage (A3, A5), alternative transcription start and termination sites (ATSS, ATTS), exon skipping (ES), intron retention (IR), mutually exclusive exons (MEE), and multiple exon skipping (MES), comparing normal and tumor samples. (b) Summary of structural and regulatory consequences associated with isoform switches, including changes in exon number, intron retention and intron structure, as well as alternative transcription start (TSS) and termination sites (TTS), comparing normal and tumor samples.

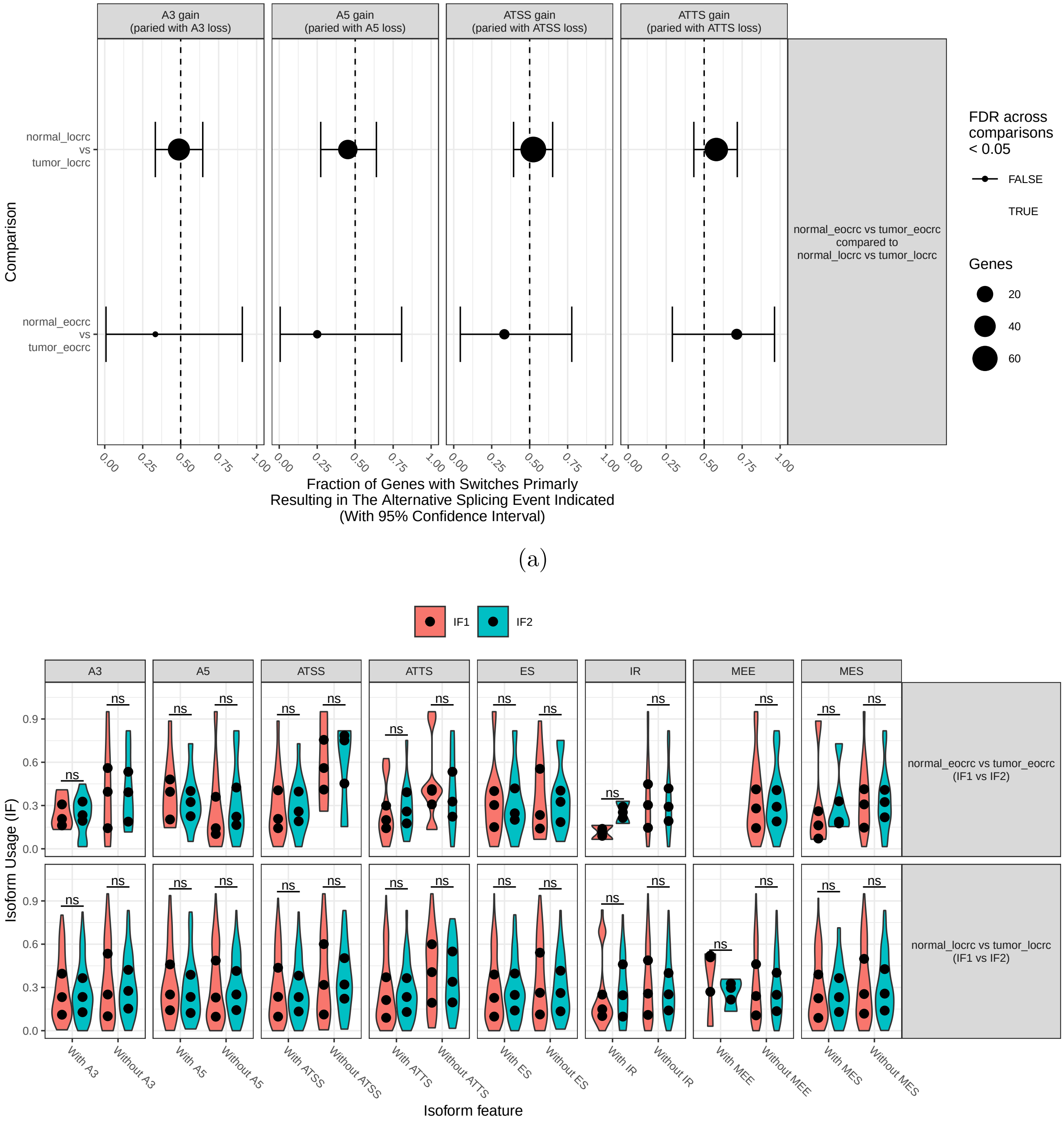

(a)

(b)

Figure 3.12: (a) Comparison of alternative splicing enrichment between EOCRC and LOCRC isoform switches, showing the proportion of splicing gains versus losses for A3, A5, ATSS, and ATTS events in *normal–tumor* contrasts; no significant differences between comparisons were detected *Fisher's exact test.* (b)Genome-wide analysis of isoform usage associated with alternative splicing events. Global distributions of isoform fraction (IF) are shown for isoforms with and without specific splicing annotations.

3.7 RNA secondary structure prediction of isoforms

The nucleotide sequences of the six isoform switches shared between the EOCRC and LOCRC cohorts were extracted using the `extractSequence` function from the `IsoformSwitchAnalyzeR` package, see Listing 3.1. The resulting DNA sequences were transcribed into RNA and secondary structure prediction was performed using *RNAStructure*, applying minimum free energy-based folding algorithms. The predicted two-dimensional RNA structures for the representative isoforms are shown in Figure 3.13 and Figure 3.14. For a more detail description of the RNA secondary structure prediction analysis, refer to the master-bioinformatics GitHub project.

To quantitatively characterize RNA structural features, the *bpRNA* tool was used to annotate and count major secondary structure elements, including bulges, hairpins, internal loops, external regions, multiloops, and stems. A heatmap representation summarizes the distribution of these structural motifs across the six shared isoforms, highlighting stems and internal loops as the most prevalent features, see Figure 3.14.

This secondary structure analysis was further extended to the ten most significant isoform switches identified independently in each cohort, see Listing D.1 and Listing D.2. Overall, a similar structural composition was observed in both EOCRC and LOCRC, with stems and internal loops remaining dominant, refer to Figure 3.15. However, cohort-specific isoforms showed an increased abundance of hairpin structures, suggesting a higher degree of local folding complexity in these transcripts.

Listing 3.1: FASTA sequences of the 6 overlapped isoforms exhibiting DTU in both EOCRC and LOCRC.

```
>ENST00000378292.9
GCGGCCGCACCCCCCGGCCGGGCCGTGCTTCTGCCCCTACAAGGTTTGGGCCGAGGTGGGGGAGGGTCCTGGTTGCCGGC

>ENST00000338983.7
CTTCCTCATTGGCGCCGTGCAGAGAGGCGGAATGTTCAACTCCTAACTGCAGCGGAAACGTGGGAGCCGCGCGGGCCGCT

>ENST00000329305.6
TCCTCCTCGCCTGCCACCGGTGCACCCAGTCCGCTCACCCAGCCCAGTCCGTCCGGTCCTCACCGCCTGCCGGCCGGCCC

>ENST00000532465.1
CCTCGGGTAGCGTCAGCATCGAGGAGATCGACCTGGAGGGCAAGTTTGTGCAGCTCAAGAACAACTCGGACAAGGATCAG

>ENST00000325327.4
ATCTTGCAGCCGGCGGCGCGGATTGAATGAGCCCGCCGAGCCCGGGCCGCCGTCGGGAGCAGCGCAGGCCGCGAGCCGCC

>ENST00000467155.7
CCCTATCCATTTGACATCTAAATGTCATAGCGACTTTTGGGATAGTTTGCTATCGACAAAGGGAGACAAAGTCAAGGGGT
```

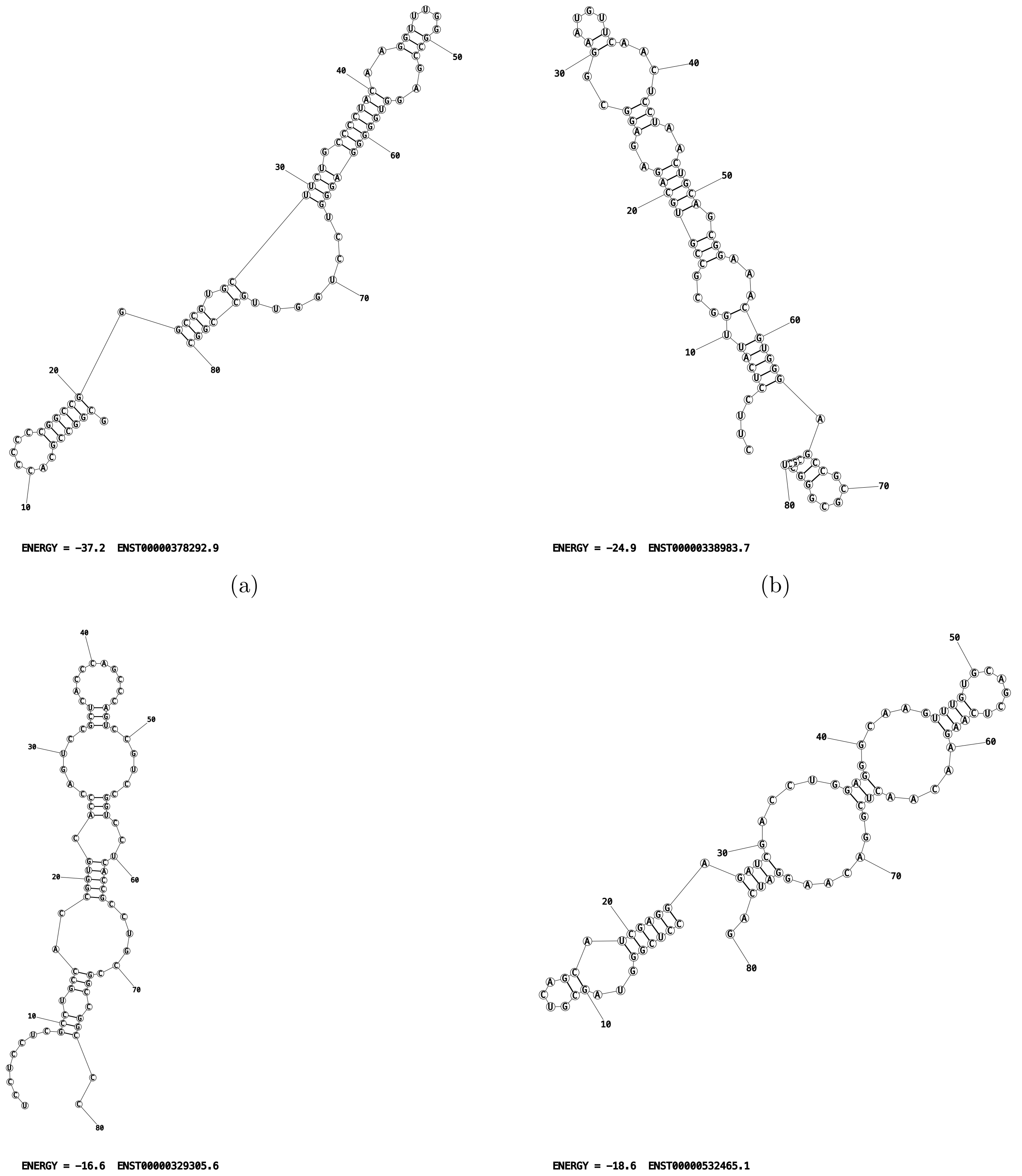
50
40
60
30
70
20
80
10
ENERGY = -37.2 ENST00000378292.9
30
40
50
20
60
10
70
80
ENERGY = -24.9 ENST00000338983.7
40
50
30
20
60
70
10
80
ENERGY = -16.6 ENST00000329305.6
50
60
40
30
70
20
80
10
ENERGY = -18.6 ENST00000532465.1

(a)

(b)

(c)

(d)

Figure 3.13: RNA secondary structure prediction of isoforms shared between EOCRC and LOCRC obtained using *RNAStructure* software. (a) *ENST00000378292.9*, (b) *ENST00000338983.7*, (c) *ENST00000329305.6*, and (d) *ENST00000532465.1*.

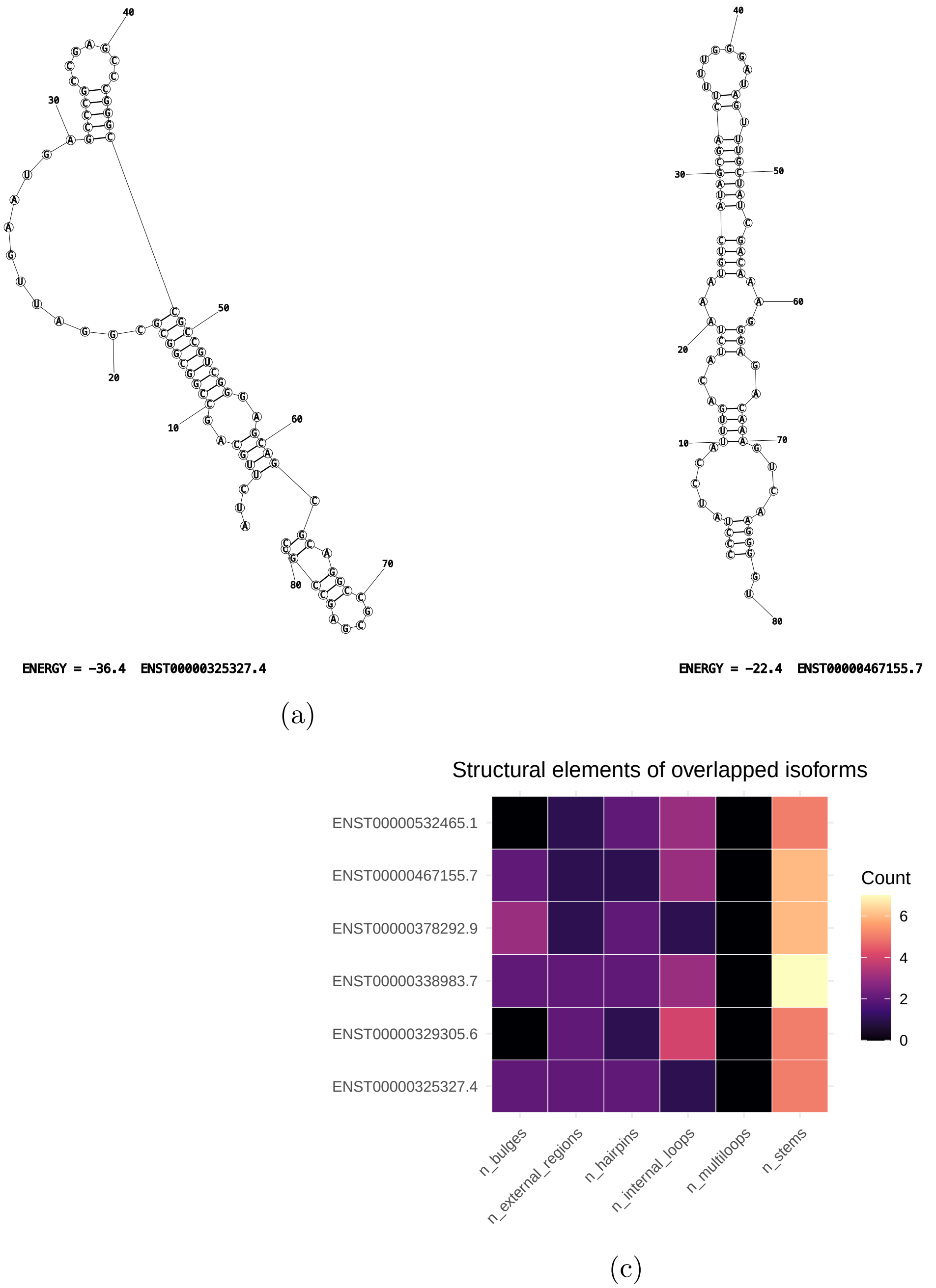

(a)

(b)

(c)

Figure 3.14: RNA secondary structure prediction of isoforms shared between EOCRC and LOCRC obtained using *RNAStructure* software. (a) *ENST00000325327.4*, (b) *ENST00000467155.7*, and (c) heatmap of RNA secondary structure motifs of the 6 shared DTU isoforms obtained using the *bpRNA* toolkit.

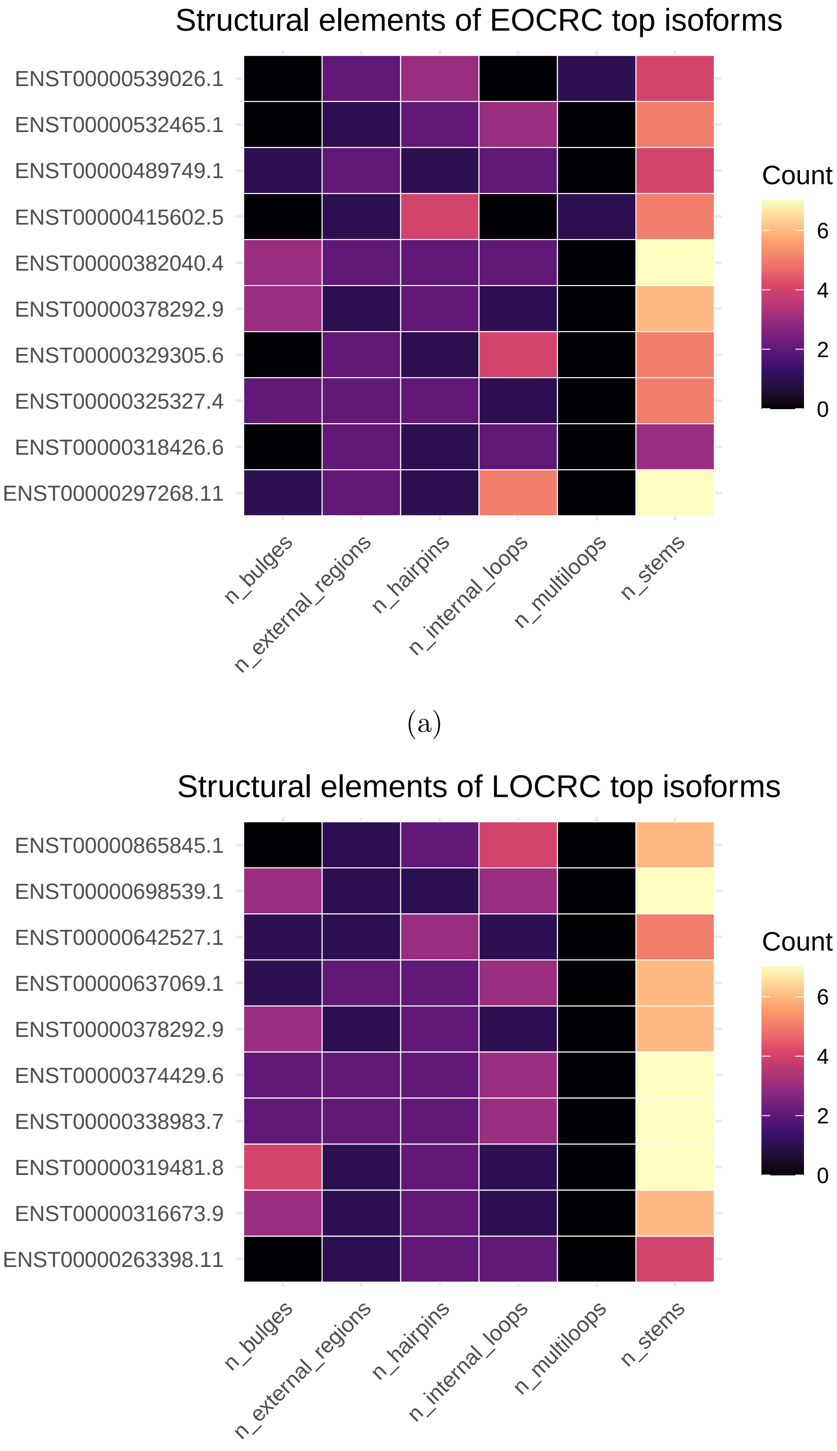

Structural elements of EOCRC top isoforms

(a)

Structural elements of LOCRC top isoforms

(b)

Figure 3.15: Heatmap of RNA secondary structure motifs of the top DTU isoforms obtained using the *bpRNA* toolkit. (a) EOCRC samples. (b) LOCRC samples.

Chapter 4

Discussion

In this work, we analyzed RNA sequencing data from patient-matched tumor and adjacent normal tissues obtained from EOCRC (n = 21) and LOCRC (n = 22) cohorts. While we identified several molecular features associated with EOCRC, including differences in gene expression, isoform usage, and alternative splicing patterns, consistent with prior reports [31, 2], we did not observe broad transcriptome-wide differences distinguishing EOCRC from LOCRC.

4.1 Differential Gene Expression Analysis

Differential gene expression analysis using *DESeq2* identified 40 genes uniquely deregulated in EOCRC. Functional enrichment analysis of these genes revealed overrepresentation of immune-related, inflammatory regulatory, and cell adhesion processes, in agreement with previous transcriptomic studies of EOCRC [32, 33]. The partial overlap between our 40-gene set and the 48 EOCRC-specific genes identified by Marx et al. [2] is because we did not apply an additional expression cutoff threshold of 1.5 LFC difference between EOCRC and LOCRC cohorts.

Although clinical and demographic variables were not explicitly modeled in our analysis, despite their known contribution to EOCRC risk [34, 35], we nonetheless recovered 4 of the 8 EOCRC-associated gene signatures curated by Marx et al. [2]. While WNT11, MSLN, and IL1RN have known roles in CRC, SLC38A11 is an understudied candidate in this context. These four genes might give insight into EOCRC pathogenesis and serve as prognostic markers compared to LOCRC based on the following information:

- **WNT11:** Activates non-canonical Wnt signaling pathways that regulate cell motility and invasion in colorectal cancer [36]. More recently, circulating WNT11 levels have been proposed as a minimally invasive biomarker for monitoring colorectal cancer liver metastases in the context of immunotherapy [37].

- **MSLN:** Its high expression in colorectal cancer is associated with immune-related features, including increased macrophage infiltration, elevated PD-L1 levels, and activation of inflammatory signaling pathways [38]. These tumors also frequently harbor KRAS and FBXW7 mutations, suggesting a link between MSLN expression, tumor progression, and immune modulation.

- **IL1RN:** Encodes the interleukin-1 receptor antagonist, a modulator of IL-1 driven inflammation in the tumor microenvironment. Disruptions in `IL-1/IL-1RN` balance are implicated in cancer-associated inflammation and immune suppression [39]. Moreover, IL1RN expression has been reported as a prognostic marker correlated with immune cell infiltration in colorectal cancer [40].

- **SLC38A11:** A gene implicated in cellular metabolic processes [41], which has been significantly associated with metastatic progression in colorectal cancer [2], suggesting potential clinical relevance in EOCRC patients.

4.2 Differential Transcript Usage Analysis

The direct comparison of the alternative splicing analysis conducted by Marx et al. [2] and our isoform-switch analysis on the same dataset, revealed that these are complementary approaches. Their splice analysis strategy with rMATS and Whippet identified a broad spectrum of splicing perturbations. In contrast, our DTU analysis with `IsoformSwitchAnalyzeR`, curated these events into a list of significant consequential isoform switches. This indicates that while splicing dysregulation is widespread in CRC, only a subset of these events led to a rewiring of the dominant gene isoform.

Moreover, we observed no overlapping between genes identified by our differential gene expression (DGE) and differential transcript usage (DTU), and event-based splicing analyses from Marx et al. [2] in both EOCRC and LOCRC cohorts. The absence of shared genes reveals that these analytical layers capture distinct aspects of transcriptome variation. This independence aligns with the understanding that changes in gene level expression profiles, isoform level expression profiles, and alternative splicing events can occur separately [42, 43, 44]. Taken together, these findings imply that analyses limited to a single transcriptomic level risk missing relevant molecular changes in colorectal cancer.

Our DTU analysis identified several genes with consistent isoform switching in both EOCRC and LOCRC cohorts, with potential relevance to colorectal cancer biology:

- **TPM2:** It was significantly downregulated at the transcript level in tumors compared with normal tissue in both EOCRC and LOCRC. While direct mechanistic evidence for TPM2 in colorectal cancer remains limited, elevated TPM2 expression in tumor-associated stromal cells was shown to outperform several established prognostic markers, indicating potential clinical relevance for patient stratification [45].

- **LMNB2:** Functional evidence indicates that LMNB2 promotes tumor cell proliferation by regulating cell cycle progression through the p21 pathway, supporting its relevance as a prognostic marker in CRC [46].

- **HOXB-AS3:** A lncRNA that encodes a conserved micropeptide that suppresses colorectal cancer growth by modulating alternative splicing of PKM and limiting metabolic reprogramming. Loss of the HOXB-AS3 peptide is associated with increased tumor progression and poorer prognosis in CRC patients [47].

- **MAP3K20:** There is currently no primary literature linking MAP3K20 to colorectal tumorigenesis. However, Marx et al. [2] identified tumor-specific splicing of a similar gene, MAP3K8 in EOCRC. Both genes belong to the larger Mitogen-Activated Protein Kinase (MAPK) pathway and function as MAP kinase kinase kinases (MAP3Ks). This suggests that dysregulation of MAP3K family members may contribute to CRC pathogenesis.

4.3 Alternative Splicing Regulation

Alternative splicing has been proposed as an important regulatory layer contributing to age-related differences in colorectal cancer. Marx et al. [2] reported a higher number of differentially spliced events in LOCRC compared to EOCRC, with exon skipping representing the dominant splicing category in both cohorts, but with substantially greater complexity in late-onset tumors. In addition, their observation that tumor and normal samples could be separated based on splice junction usage suggests that alternative splicing contributes to the transcriptomic differences between EOCRC and LOCRC.

Our results, obtained through DTU analysis, are consistent with these observations and extend them at the isoform level. While the analytical frameworks differ, both approaches agree that LOCRC tumors exhibit a more extensive splicing perturbation than EOCRC tumors. In our analysis, exon skipping, alternative splice site usage, and other transcript-level alterations affected a higher number of isoforms in LOCRC, whereas EOCRC tumors showed only limited involvement across all splicing categories.

4.4 RNA Secondary Structure Analysis

Canonical RNA secondary structures including hairpins, stems, bulges, internal loops, and loops are fundamental determinants of RNA function [15], representing an additional regulatory layer beyond nucleotide sequence and gene level expression. In our study, We extended our DTU analysis to examine the RNA secondary structure of key isoforms, asking whether structural differences could distinguish EOCRC from LOCRC transcriptomes.

While we observed a general enrichment of stem motifs across isoforms, a cohort-specific structural signature was not identified. This was because we used little data to make these predictions. Nonetheless, this work provides a necessary framework for future, large-scale studies. This is critical because secondary structure can be a direct target for intervention. For instance, Liu et al. [48] demonstrated that specific motifs in microRNA precursors provide a rationale for designing small molecules to interfere with their maturation, a strategy that could be adapted to target oncogenic isoforms in CRC. Thus, our pipeline lays the groundwork for identifying such targetable structures in crc-associated transcripts.

Chapter 5

Conclusions and future works

Our study implemented an integrative transcriptomic framework to characterize molecular differences between early-onset and late-onset colorectal cancer, combining differential gene expression, differential transcript usage, and RNA secondary structure prediction. This multilayered approach revealed age-associated heterogeneity that is not captured by gene-level analyses alone.

A central finding was the identification of a 40-gene signature uniquely deregulated in EOCRC, mainly enriched in immune-related processes. The involvement of genes such as WNT11, MSLN, IL1RN, and SLC38A11 supported the existence of a distinct molecular and immune microenvironment in early-onset disease.

Isoform-level analysis uncovered pronounced differences in post-transcriptional regulation between cohorts. Late-onset tumors exhibited extensive transcriptome remodeling with hundreds of isoform switches, whereas early-onset tumors showed a comparatively constrained splicing landscape. Despite these global differences, six recurrent isoform switches were shared between cohorts, including TPM2, LMNB2, MAP3K20, and the long non-coding RNA HOXB-AS3.

RNA secondary structure prediction revealed a general enrichment of stem motifs among significant isoforms, establishing a computational pipeline for incorporating structural features into transcriptomic analyses. Although age-specific structural signatures were not conclusively identified, this framework provides a foundation for future large-scale studies.

Overall, the results demonstrate that integrative bioinformatics strategies are essential for capturing transcriptomic complexity and highlight potential molecular candidates relevant to early detection and personalized therapeutic approaches in colorectal cancer.

5.1 Planning Follow-up

The execution of this project faced several technical and methodological challenges that required continuous monitoring and adaptive decision-making. Progress was tracked against predefined milestones using a dedicated GitHub project board, which enabled transparent documentation of changes in scope and analytical strategy. A major risk identified during development was the infeasibility of deploying RiNALMo, an RNA large language models for secondary structure prediction, due to GPU memory and architecture constraints on the available infrastructure at the University of Navarra. This limitation necessitated a revision of the original project scope and a methodological pivot toward thermodynamics-based RNA structure prediction using *RNAStructure*. Additional risks related to biological interpretability were mitigated by anchoring downstream structural analyses to high-confidence candidates derived from differential gene expression and differential transcript usage analyses. These mitigation strategies ensured that, despite infrastructure constraints and analytical complexity, all core objectives were achieved within the planned timeline.

5.2 Improvements and Future Work

As future work, we propose to perform differential transcript usage analysis using the nf-core/rnasplice pipeline as an alternative to the manual approach based on `IsoformSwitchAnalyzeR`. This comparison would allow the assessment of result consistency while improving reproducibility through the use of a standardized and community-maintained workflow. The `nf-core/rnasplice` pipeline is a relatively recent tool whose adoption has steadily increased, making it a robust option for large-scale alternative splicing analyses.

The combined use of multiple `Nextflow`-based pipelines enables the coherent integration of differential gene expression (DGE) and differential transcript usage (DTU) analyses. In this context, a relevant improvement would be the automation of nucleotide sequence extraction from the most significant isoform switches, followed by the incorporation of an additional module for RNA secondary structure prediction. Since `Nextflow` constitutes the core processing framework, this integration could be implemented through auxiliary scripts, such as `Bash` or `Python`, allowing the construction of a unified workflow encompassing DGE, DTU, and RNA secondary structure analyses.

Furthermore, the current workflow could be extended by incorporating public RNA-seq data from one of the most comprehensive studies conducted to date in colorectal cancer, *Prognostic genome and transcriptome signatures in colorectal cancers* [49]. This study includes RNA-seq data from 1183 colorectal cancer patients. The main objective of this extension would be to identify a larger number of isoform switches, particularly involving non-coding RNAs, with potential value as biomarkers for early-onset colorectal cancer, thereby contributing to a deeper understanding of the molecular mechanisms underlying disease pathogenesis.

Finally, future efforts could focus on exploring state-of-the-art computational approaches, such as large language models for RNA such as RiNALMo, whose application to RNA secondary structure prediction has recently gained significant attention within the scientific community. In this context, we aim to reproduce and integrate methodologies described in recent benchmarking studies, such as *Comprehensive benchmarking of large language models for RNA secondary structure prediction* [23], once access to the computational infrastructure provided by the EuroCC Spain Testbed becomes available.

Chapter 6

Glossary

Colorectal Cancer (CRC) One of the leading causes of global cancer-related mortality and morbidity, traditionally associated with older populations.

Early-Onset Colorectal Cancer (EOCRC) A subtype of colorectal cancer diagnosed in individuals younger than 50 years, often exhibiting distinct clinical, molecular, and prognostic characteristics.

Late-Onset Colorectal Cancer (LOCRC) Colorectal cancer diagnosed in individuals older than 50 years, used in this study as a reference cohort for identifying age-associated molecular differences.

Transcriptome The complete set of RNA transcripts produced by the genome, commonly analyzed using RNA sequencing to identify dysregulated pathways and candidate biomarkers.

Differential Gene Expression (DGE) A statistical analysis used to identify genes with significant changes in overall expression levels between biological conditions, such as tumor and normal tissues.

Differential Transcript Usage (DTU) An analytical approach that detects changes in the relative usage of transcript isoforms between conditions, independent of total gene expression.

Alternative Splicing A post-transcriptional regulatory mechanism that produces multiple mRNA isoforms from a single gene, contributing to functional and proteomic diversity.

Isoform Switch An event in which the dominant transcript isoform of a gene differs between biological conditions, potentially altering gene function.

RNA Secondary Structure (RSS) The two-dimensional folding patterns adopted by RNA molecules, which influence their stability, interactions, and biological function beyond nucleotide sequence.

Minimum Free Energy (MFE) A thermodynamic principle used in computational RNA folding to predict the most stable RNA conformation.

Pseudo-alignment A computational method for estimating transcript abundance by mapping sequencing reads to a transcriptome index rather than performing full genomic alignment.

Gene Ontology (GO) Enrichment A statistical method used to identify biological processes, molecular functions, or cellular components that are overrepresented in a given gene set.

Structural Motifs Discrete elements of RNA secondary structure, including stems, hairpins, bulges, and internal loops, used to characterize RNA structural complexity.

Long Non-coding RNA (lncRNA) RNA transcripts longer than 200 nucleotides that do not encode proteins but play important regulatory roles in gene expression and cellular processes.

Bibliography

[1] Bert Vogelstein, Nickolas Papadopoulos, Victor E. Velculescu, Shibin Zhou, Luis A. Diaz, and Kenneth W. Kinzler. Cancer genome landscapes. *Science (New York, N.Y.)*, 339(6127):1546–1558, March 2013.

[2] Olivia M. Marx, Marc M. Mankarious, Walter A. Koltun, and Gregory S. Yochum. Identification of differentially expressed genes and splicing events in early-onset colorectal cancer. *Frontiers in Oncology*, 14, April 2024.

[3] Alexandra N. Willauer, Yusha Liu, Allan A. L. Pereira, Michael Lam, Jeffrey S. Morris, Kanwal P. S. Raghav, Van K. Morris, David Menter, Russell Broaddus, Funda Meric-Bernstam, Andrea Hayes-Jordan, Winston Huh, Michael J. Overman, Scott Kopetz, and Jonathan M. Loree. Clinical and molecular characterization of early-onset colorectal cancer. *Cancer*, 125(12):2002–2010, 2019.

[4] Andrea N. Burnett-Hartman, J. David Powers, Jessica Chubak, Douglas A. Corley, Nirupa R. Ghai, Carmit K. McMullen, Pamala A. Pawloski, Andrew T. Sterrett, and Heather Spencer Feigelson. Treatment patterns and survival differ between early-onset and late-onset colorectal cancer patients: The patient outcomes to advance learning network. *Cancer Causes & Control*, 30(7):747–755, July 2019.

[5] Ting Xu, Yinjie Zhang, Jing Zhang, Changsong Qi, Dan Liu, Zhenghang Wang, Yanyan Li, Congcong Ji, Jian Li, Xuan Lin, Ting Hou, Hao Liu, Lu Zhang, Han Han-Zhang, Lin Shen, and Xicheng Wang. Germline Profiling and Molecular Characterization of Early Onset Metastatic Colorectal Cancer. *Frontiers in Oncology*, 10, October 2020.

[6] Litika Vermani, Rajeev Kumar, Rengaswamy R Kannan, Monoj K Deka, Anuradha Talukdar, and Nachimuthu S Kumar. Expression Pattern of Aldh1, E-Cadherin, Vimentin and Twist in Early and Late Onset Sporadic Colorectal Cancer. *Biomarkers in Medicine*, 14(14):1371–1382, October 2020.

[7] Katherine M. Watson, Ivy H. Gardner, Raphael M. Byrne, Rebecca R. Ruhl, Christian P. Lanciault, Elizabeth N. Dewey, Sudarshan Anand, and Vassiliki Liana Tsikitis. Differential Expression of PEG10 Contributes to Aggressive Disease in Early Versus Late-Onset Colorectal Cancer. *Diseases of the Colon & Rectum*, 63(12):1610, December 2020.

[8] Ye Jin Ha, Yun Jae Shin, Ka Hee Tak, Jong Lyul Park, Jeong Hwan Kim, Jong Lyul Lee, Yong Sik Yoon, Chan Wook Kim, Seon Young Kim, and Jin Cheon Kim. Reduced expression of alanyl aminopeptidase is a robust biomarker of non-familial adenomatous polyposis

and non-hereditary nonpolyposis colorectal cancer syndrome early-onset colorectal cancer. *Cancer Medicine*, 12(8):10091–10104, 2023.

[9] Helen H. N. Yan, Hoi Cheong Siu, Siu Lun Ho, Sarah S. K. Yue, Yang Gao, Wai Yin Tsui, Dessy Chan, April S. Chan, Jason W. H. Wong, Alice H. Y. Man, Bernard C. H. Lee, Annie S. Y. Chan, Anthony K. W. Chan, Ho Sang Hui, Arthur K. L. Cheung, Wai Lun Law, Oswens S. H. Lo, Siu Tsan Yuen, Hans Clevers, and Suet Yi Leung. Organoid cultures of early-onset colorectal cancers reveal distinct and rare genetic profiles. December 2020.

[10] Olivia Marx, Marc Mankarious, and Gregory Yochum. Molecular genetics of early-onset colorectal cancer. *World Journal of Biological Chemistry*, 14(2):13–27, March 2023.

[11] Adam E. Hall, Sebastian Öther-Gee Pohl, Patrizia Cammareri, Stuart Aitken, Nicholas T. Younger, Michela Raponi, Caroline V. Billard, Alfonso Bolado Carrancio, Aslihan Bastem, Paz Freile, Fiona Haward, Ian R. Adams, Javier F. Caceres, Paula Preyzner, Alex von Kriegsheim, Malcolm G. Dunlop, Farhat V. Din, and Kevin B. Myant. RNA splicing is a key mediator of tumour cell plasticity and a therapeutic vulnerability in colorectal cancer. *Nature Communications*, 13(1):2791, May 2022.

[12] Malini Bhadra, Porsha Howell, Sneha Dutta, Caroline Heintz, and William B. Mair. Alternative splicing in aging and longevity. *Human Genetics*, 139(3):357–369, March 2020.

[13] Nancy Martínez-Montiel, Nora Hilda Rosas-Murrieta, Mónica Martínez-Montiel, Mayra Patricia Gaspariano-Cholula, and Rebeca D. Martínez-Contreras. Microbial and Natural Metabolites That Inhibit Splicing: A Powerful Alternative for Cancer Treatment. *BioMed Research International*, 2016(1):3681094, 2016.

[14] Kristoffer Vitting-Seerup and Albin Sandelin. IsoformSwitchAnalyzeR: Analysis of changes in genome-wide patterns of alternative splicing and its functional consequences. *Bioinformatics*, 35(21):4469–4471, November 2019.

[15] Xinang Cao, Yueying Zhang, Yiliang Ding, and Yue Wan. Identification of RNA structures and their roles in RNA functions. *Nature Reviews Molecular Cell Biology*, 25(10):784–801, October 2024.

[16] Jessica S. Reuter and David H. Mathews. RNAstructure: Software for RNA secondary structure prediction and analysis. *BMC Bioinformatics*, 11(1):129, March 2010.

[17] Ronny Lorenz, Stephan H. Bernhart, Christian Höner zu Siederdissen, Hakim Tafer, Christoph Flamm, Peter F. Stadler, and Ivo L. Hofacker. ViennaRNA Package 2.0. *Algorithms for Molecular Biology*, 6(1):26, November 2011.

[18] Ivo L. Hofacker, Martin Fekete, and Peter F. Stadler. Secondary Structure Prediction for Aligned RNA Sequences. *Journal of Molecular Biology*, 319(5):1059–1066, June 2002.

[19] Stefan Washietl, Ivo L. Hofacker, and Peter F. Stadler. Fast and reliable prediction of noncoding RNAs. *Proceedings of the National Academy of Sciences*, 102(7):2454–2459, February 2005.

[20] Elena Rivas, Jody Clements, and Sean R. Eddy. A statistical test for conserved RNA structure shows lack of evidence for structure in lncRNAs. *Nature Methods*, 14(1):45–48, January 2017.

[21] Kengo Sato and Michiaki Hamada. Recent trends in RNA informatics: A review of machine learning and deep learning for RNA secondary structure prediction and RNA drug discovery. *Briefings in Bioinformatics*, 24(4):bbad186, July 2023.

[22] Anqi Lin, Junpu Ye, Chang Qi, Lingxuan Zhu, Weiming Mou, Wenyi Gan, Dongqiang Zeng, Bufu Tang, Mingjia Xiao, Guangdi Chu, Shengkun Peng, Hank Z H Wong, Lin Zhang, Hengguo Zhang, Xinpei Deng, Kailai Li, Jian Zhang, Aimin Jiang, Zhengrui Li, and Peng Luo. Bridging artificial intelligence and biological sciences: A comprehensive review of large language models in bioinformatics. *Briefings in Bioinformatics*, 26(4):bbaf357, July 2025.

[23] Luciano I Zablocki, Leandro A Bugnon, Matias Gerard, Leandro Di Persia, Georgina Stegmayer, and Diego H Milone. Comprehensive benchmarking of large language models for RNA secondary structure prediction. *Briefings in Bioinformatics*, 26(2):bbaf137, March 2025.

[24] Rasko Leinonen, Hideaki Sugawara, Martin Shumway, and on behalf of the International Nucleotide Sequence Database Collaboration. The Sequence Read Archive. *Nucleic Acids Research*, 39(suppl_1):D19–D21, January 2011.

[25] Philip A. Ewels, Alexander Peltzer, Sven Fillinger, Harshil Patel, Johannes Alneberg, Andreas Wilm, Maxime Ulysse Garcia, Paolo Di Tommaso, and Sven Nahnsen. The nf-core framework for community-curated bioinformatics pipelines. *Nature Biotechnology*, 38(3):276–278, March 2020.

[26] Rob Patro, Geet Duggal, Michael I. Love, Rafael A. Irizarry, and Carl Kingsford. Salmon provides fast and bias-aware quantification of transcript expression. *Nature Methods*, 14(4):417–419, April 2017.

[27] Michael I. Love, Wolfgang Huber, and Simon Anders. Moderated estimation of fold change and dispersion for RNA-seq data with DESeq2. *Genome Biology*, 15(12):550, December 2014.

[28] Tianzhi Wu, Erqiang Hu, Shuangbin Xu, Meijun Chen, Pingfan Guo, Zehan Dai, Tingze Feng, Lang Zhou, Wenli Tang, Li Zhan, Xiaocong Fu, Shanshan Liu, Xiaochen Bo, and Guangchuang Yu. clusterProfiler 4.0: A universal enrichment tool for interpreting omics data. *The Innovation*, 2(3):100141, August 2021.

[29] Simon Anders, Alejandro Reyes, and Wolfgang Huber. Detecting differential usage of exons from RNA-seq data. *Genome Research*, 22(10):2008–2017, January 2012.

[30] Padideh Danaee, Mason Rouches, Michelle Wiley, Dezhong Deng, Liang Huang, and David Hendrix. bpRNA: Large-scale automated annotation and analysis of RNA secondary structure. *Nucleic Acids Research*, 46(11):5381–5394, June 2018.

[31] Can Lu, Xiaopeng Zhang, Josefine Schardey, Ulrich Wirth, Kathrin Heinrich, Luca Massiminio, Giulia Martina Cavestro, Jens Neumann, Alexandr V. Bazhin, Jens Werner, and Florian Kühn. Molecular characteristics of microsatellite stable early-onset colorectal cancer as predictors of prognosis and immunotherapeutic response. *npj Precision Oncology*, 7(1):63, July 2023.

[32] Ivy H Gardner, Ragavan Siddharthan, Katherine Watson, Elizabeth Dewey, Rebecca Ruhl, Sokchea Khou, Xiangnan Guan, Zheng Xia, V Liana Tsikitis, and Sudarshan Anand. A Distinct Innate Immune Signature of Early Onset Colorectal Cancer. *ImmunoHorizons*, 5(6):489–499, June 2021.

[33] Mulong Du, Dongying Gu, Junyi Xin, Ulrike Peters, Mingyang Song, Guoshuai Cai, Shuwei Li, Shuai Ben, Yixuan Meng, Haiyan Chu, Lianmin Chen, Qianghu Wang, Lingjun Zhu, Zan Fu, Zhengdong Zhang, and Meilin Wang. Integrated multi-omics approach to distinct molecular characterization and classification of early-onset colorectal cancer. *Cell Reports Medicine*, 4(3):100974, March 2023.

[34] Cheng Kong, Lei Liang, Guang Liu, Lutao Du, Yongzhi Yang, Jianqiang Liu, Debing Shi, Xinxiang Li, and Yanlei Ma. Integrated metagenomic and metabolomic analysis reveals distinct gut-microbiome-derived phenotypes in early-onset colorectal cancer. *Gut*, 72(6):1129–1142, June 2023.

[35] Xiaobin Zheng, Jinhee Hur, Long H Nguyen, Jie Liu, Mingyang Song, Kana Wu, Stephanie A Smith-Warner, Shuji Ogino, Walter C Willett, Andrew T Chan, Edward Giovannucci, and Yin Cao. Comprehensive Assessment of Diet Quality and Risk of Precursors of Early-Onset Colorectal Cancer. *JNCI: Journal of the National Cancer Institute*, 113(5):543–552, May 2021.

[36] Irantzu Gorroño-Etxebarria, Urko Aguirre, Saray Sanchez, Nerea González, Antonio Escobar, Ignacio Zabalza, José Maria Quintana, Maria dM Vivanco, Jonathan Waxman, and Robert M. Kypta. Wnt-11 as a Potential Prognostic Biomarker and Therapeutic Target in Colorectal Cancer. *Cancers*, 11(7):908, June 2019.

[37] Weiliang Jiang, Bingjie Guan, Hongcheng Sun, Yushuai Mi, Sanjun Cai, Rong Wan, Xinxiang Li, Peng Lian, Dawei Li, and Senlin Zhao. WNT11 Promotes immune evasion and resistance to Anti-PD-1 therapy in liver metastasis. *Nature Communications*, 16(1):1429, February 2025.

[38] Midhun Malla, Sachin Kumar Deshmukh, Sharon Wu, Timothy Samec, Dane C. Olevian, Reima El Naili, Bassel El-Rayes, Joanne Xiu, Alex Farrell, Heinz-Josef Lenz, Emil Lou, Sanjay Goel, David Spetzler, Richard M. Goldberg, and Lori Hazlehurst. Mesothelin expression correlates with elevated inhibitory immune activity in patients with colorectal cancer. *Cancer Gene Therapy*, 31(10):1547–1558, October 2024.

[39] Alberto Mantovani, Isabella Barajon, and Cecilia Garlanda. IL-1 and IL-1 regulatory pathways in cancer progression and therapy. *Immunological Reviews*, 281(1):57–61, 2018.

[40] Qi Wang, Xufeng Huang, Shujing Zhou, Yuntao Ding, Huizhi Wang, Weiye Jiang, and Min Xu. IL1RN and PRRX1 as a Prognostic Biomarker Correlated with Immune Infiltrates in Colorectal Cancer: Evidence from Bioinformatic Analysis. *International Journal of Genomics*, 2022(1):2723264, 2022.

[41] Celine Garrett, Daniel Steffens, Michael Solomon, and Cherry Koh. Early-onset colorectal cancer: Why it should be high on our list of differentials. *ANZ Journal of Surgery*, 92(7-8):1638–1643, 2022.

[42] ZhongFa Zhang, Sharmistha Pal, Yingtao Bi, Julia Tchou, and Ramana V. Davuluri. Isoform level expression profiles provide better cancer signatures than gene level expression profiles. *Genome Medicine*, 5(4):33, April 2013.

[43] Gabriela A Merino, Ana Conesa, and Elmer A Fernández. A benchmarking of workflows for detecting differential splicing and differential expression at isoform level in human RNA-seq studies. *Briefings in Bioinformatics*, 20(2):471–481, March 2019.

[44] Peter A. Innes, April M. Goebl, Chris C. R. Smith, Kaylee Rosenberger, and Nolan C. Kane. Gene expression and alternative splicing contribute to adaptive divergence of ecotypes. *Heredity*, 132(3):120–132, March 2024.

[45] Valentina Mele, Camilla Basso, Valeria Governa, Jesus F. Glaus Garzon, Manuele G. Muraro, Silvio Däster, Christian A. Nebiker, Robert Mechera, Martin Bolli, Alexander Schmidt, Roger Geiger, Giulio C. Spagnoli, Dimitri Christoforidis, Pietro E. Majno, Lubor Borsig, and Giandomenica Iezzi. Identification of TPM2 and CNN1 as Novel Prognostic Markers in Functionally Characterized Human Colon Cancer-Associated Stromal Cells. *Cancers*, 14(8):2024, January 2022.

[46] Chen-Hua Dong, Tao Jiang, Hang Yin, Hu Song, Yi Zhang, Hao Geng, Pei-Cong Shi, Yi-Xin Xu, Hong Gao, Lian-Yu Liu, Lei Zhou, Zhao-Hui Zhang, and Jun Song. LMNB2 promotes the progression of colorectal cancer by silencing p21 expression. *Cell Death & Disease*, 12(4):331, March 2021.

[47] Jin-Zhou Huang, Min Chen, De Chen, Xing-Cheng Gao, Song Zhu, Hongyang Huang, Min Hu, Huifang Zhu, and Guang-Rong Yan. A Peptide Encoded by a Putative lncRNA HOXB-AS3 Suppresses Colon Cancer Growth. *Molecular Cell*, 68(1):171–184.e6, October 2017.

[48] Biao Liu, Jessica L. Childs-Disney, Brent M. Znosko, Dan Wang, Mohammad Fallahi, Steven M. Gallo, and Matthew D. Disney. Analysis of secondary structural elements in human microRNA hairpin precursors. *BMC Bioinformatics*, 17(1):112, March 2016.

[49] Luís Nunes, Fuqiang Li, Meizhen Wu, Tian Luo, Klara Hammarström, Emma Torell, Ingrid Ljuslinder, Artur Mezheyeuski, Per-Henrik Edqvist, Anna Löfgren-Burström, Carl Zingmark, Sofia Edin, Chatarina Larsson, Lucy Mathot, Erik Osterman, Emerik Osterlund, Viktor Ljungström, Inês Neves, Nicole Yacoub, Unnur Gudnadóttir, Helgi Birgisson, Malin Enblad, Fredrik Ponten, Richard Palmqvist, Xun Xu, Mathias Uhlén, Kui Wu, Bengt Glimelius, Cong Lin, and Tobias Sjöblom. Prognostic genome and transcriptome signatures in colorectal cancers. *Nature*, 633(8028):137–146, September 2024.

Appendix A

EOCRC supplementary figures and tables

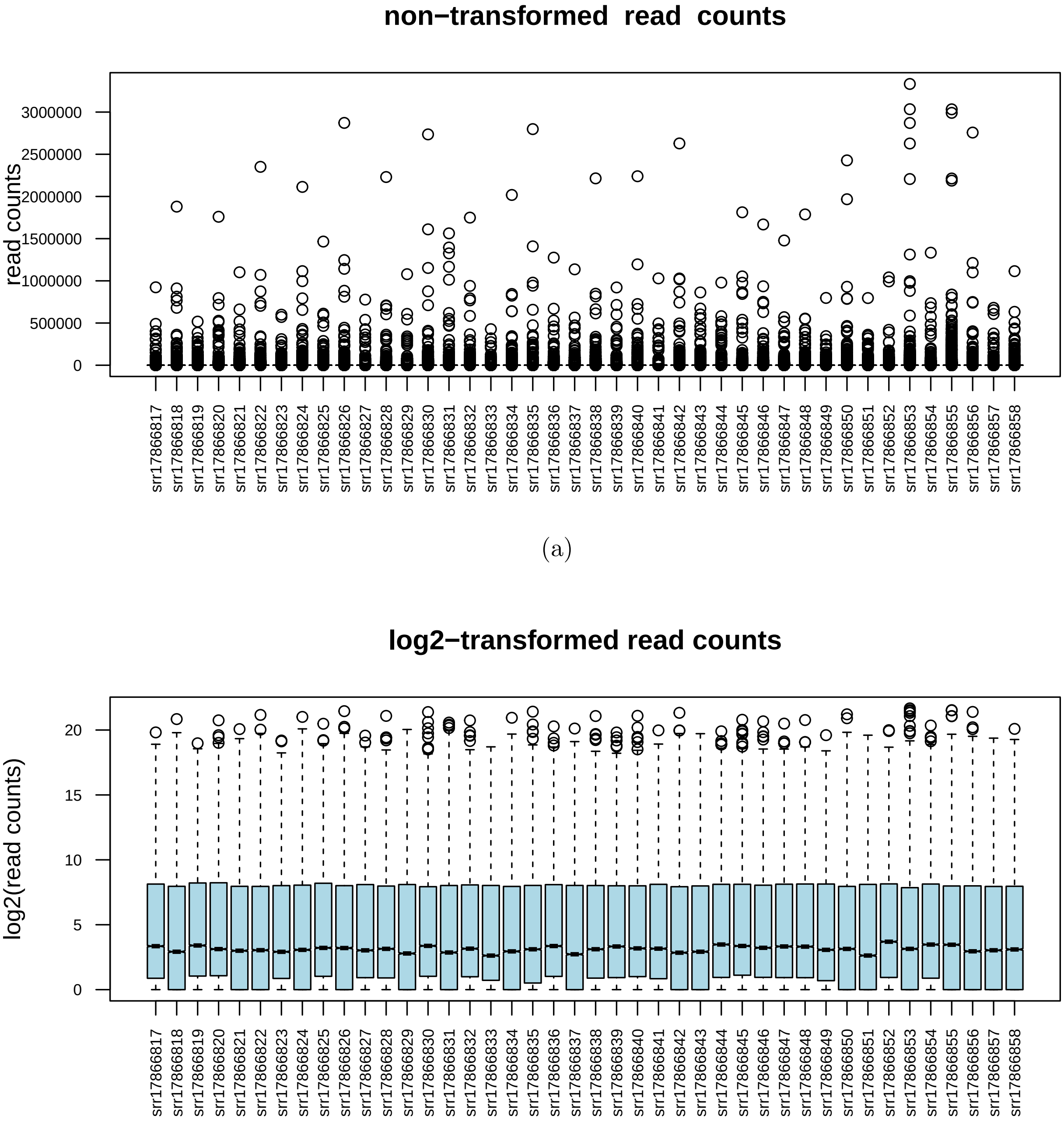

(a)

(b)

Figure A.1: EOCRC samples (a) Normalized counts before log2 transformation. (b) Normalized counts after log2 transformation.

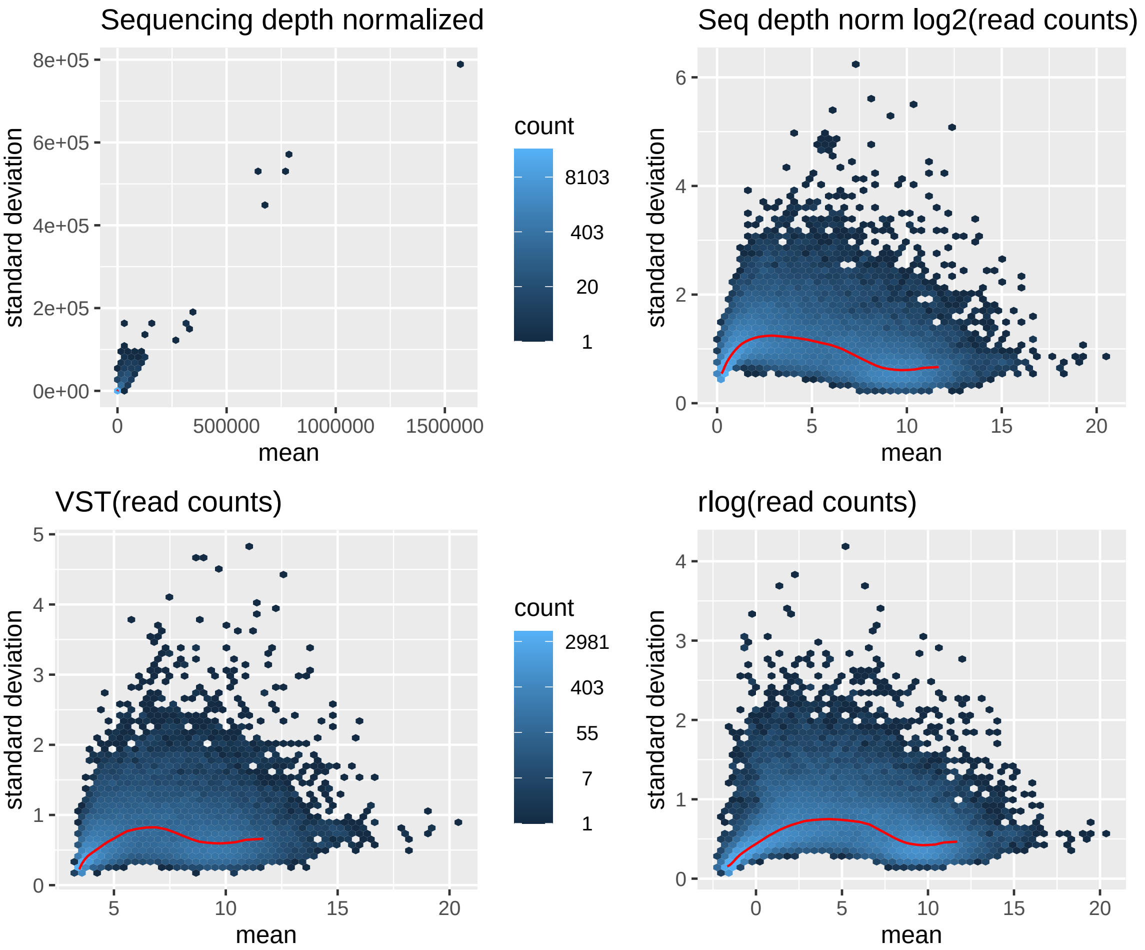

Figure A.2: Comparison of different normalization and data transformation methods for EOCRC samples. (a) Raw counts before normalization. (b) Normalized counts after sequencing depth normalization. (c) Normalized counts after variance stabilizing transformation (vst). (d) Normalized counts after regularized log transformation (rlog).

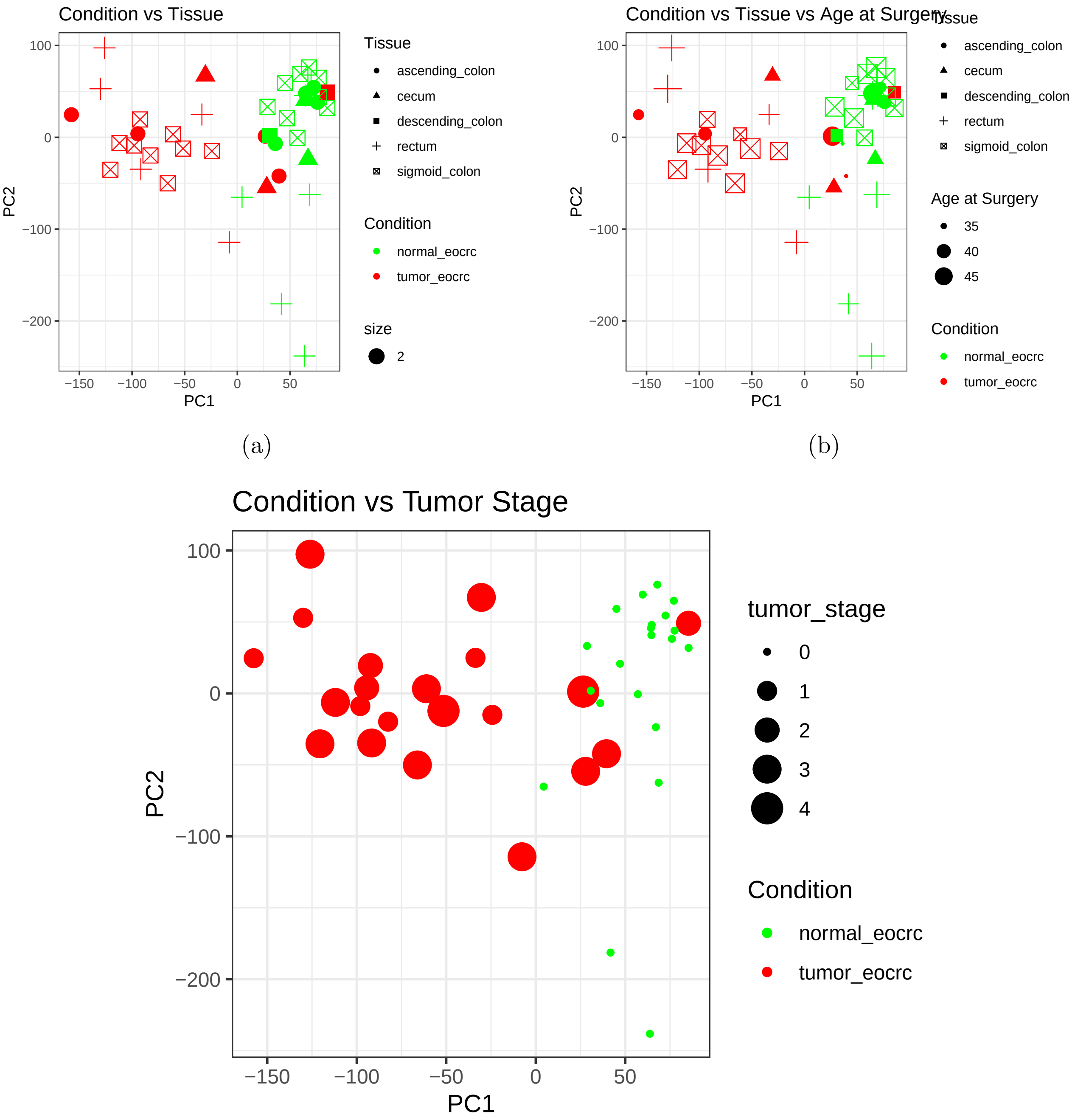

(a)

(b)

(c)

Figure A.3: PCA of EOCRC samples based on `condition & tissue`, `condition & tissue & age at surgery`, `condition & tumor stage`.

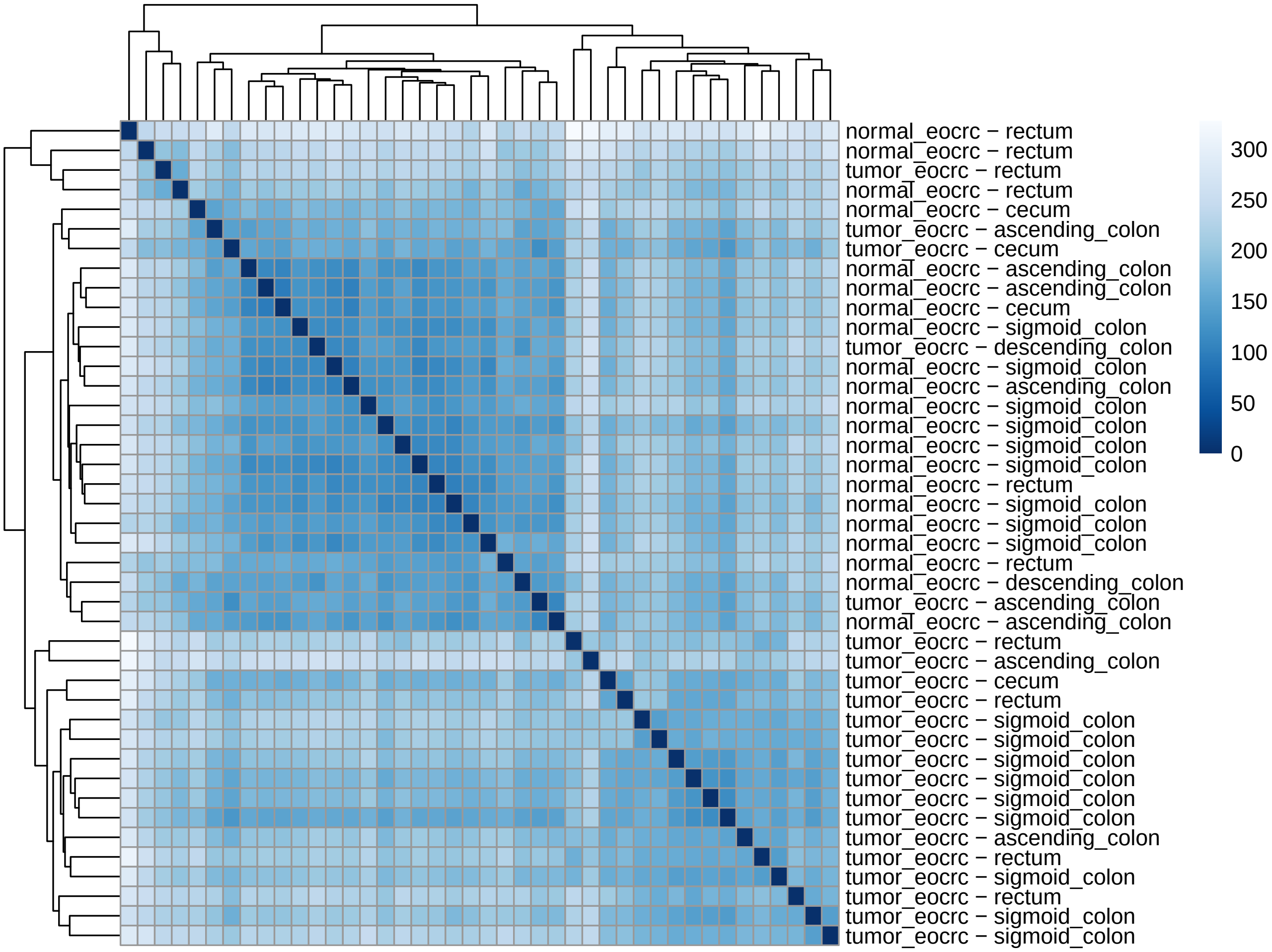

Figure A.4: Distance heatmap of EOCRC samples based on variance stabilizing transformation (vst) normalized counts. The heatmap displays hierarchical clustering of samples, with color intensity representing the distance between sample expression profiles.

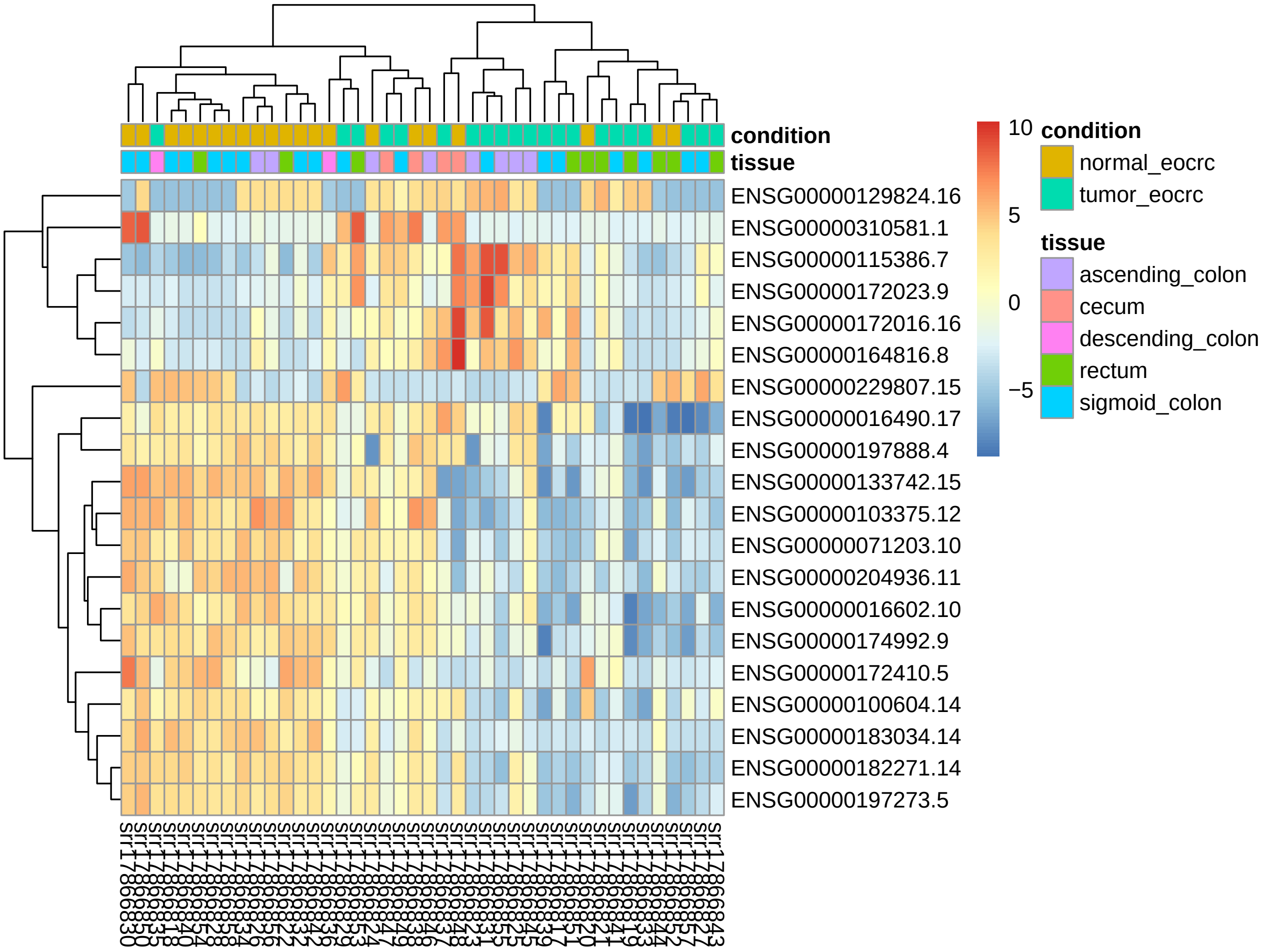

Figure A.5: Hierachical heatmap of EOCRC samples.

Table A.1: Top DEGs of the EOCRC cohort.

	Gene	baseMean	log2FoldChange	padj
ENSG00000105464	GRIN2D	140.9	4.173	1.92e-27
ENSG00000164283	ESM1	109.8	5.233	1.32e-26
ENSG00000175832	ETV4	726.7	4.371	5.78e-24
ENSG00000107159	CA9	388.8	5.637	1.03e-20
ENSG00000163347	CLDN1	625.0	4.503	1.03e-20
ENSG00000170373	CST1	396.6	7.035	1.03e-20
ENSG00000172031	EPHX4	75.8	4.433	1.03e-20
ENSG00000236081	ELFN1-AS1	137.8	4.789	1.03e-20
ENSG00000111110	PPM1H	322.7	2.141	1.36e-20
ENSG00000172164	SNTB1	362.7	2.083	3.14e-20
ENSG00000108244	KRT23	683.8	6.429	6.29e-20
ENSG00000181577	LINC03040	230.7	4.475	1.71e-19
ENSG00000178773	CPNE7	219.2	4.129	2.29e-19
ENSG00000164379	FOXQ1	402.9	4.316	8.63e-19
ENSG00000143412	ANXA9	57.7	4.183	3.24e-18
ENSG00000101255	TRIB3	475.7	3.205	4.92e-18
ENSG00000006071	ABCC8	18.9	-3.287	6.02e-18
ENSG00000015413	DPEP1	2447.4	5.143	1.27e-17
ENSG00000050344	NFE2L3	1521.0	2.459	1.85e-17
ENSG00000162073	PAQR4	567.1	2.020	1.93e-17
ENSG00000100505	TRIM9	55.1	-3.364	6.88e-17
ENSG00000171951	SCG2	298.4	-3.263	7.52e-17
ENSG00000103021	CFAP263	134.0	2.198	8.55e-17
ENSG00000173894	CBX2	108.6	3.503	8.62e-17
ENSG00000104237	RP1	21.6	5.431	2.20e-16
ENSG00000034971	MYOC	22.4	-4.999	2.40e-16
ENSG00000281406	BLACAT1	93.9	4.173	2.61e-16
ENSG00000212993	POU5F1B	95.9	4.010	3.62e-16
ENSG00000245694	CRNDE	65.3	3.435	5.01e-16
ENSG00000129474	AJUBA	156.1	2.731	8.76e-16

Appendix B

LOCRC supplementary figures and tables

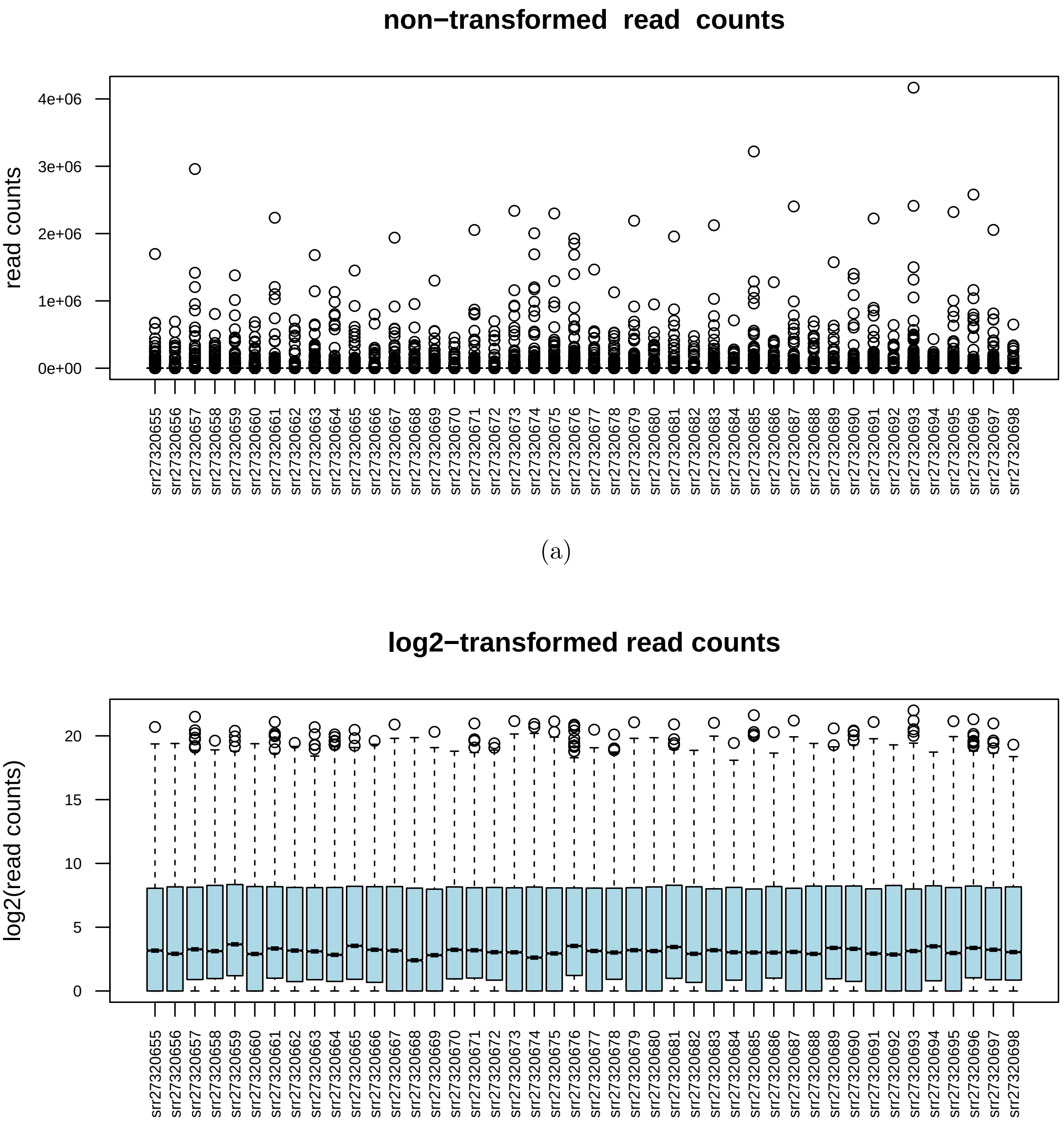

(a)

(b)

Figure B.1: LOCRC samples (a) Normalized counts before log2 transformation. (b) Normalized counts after log2 transformation.

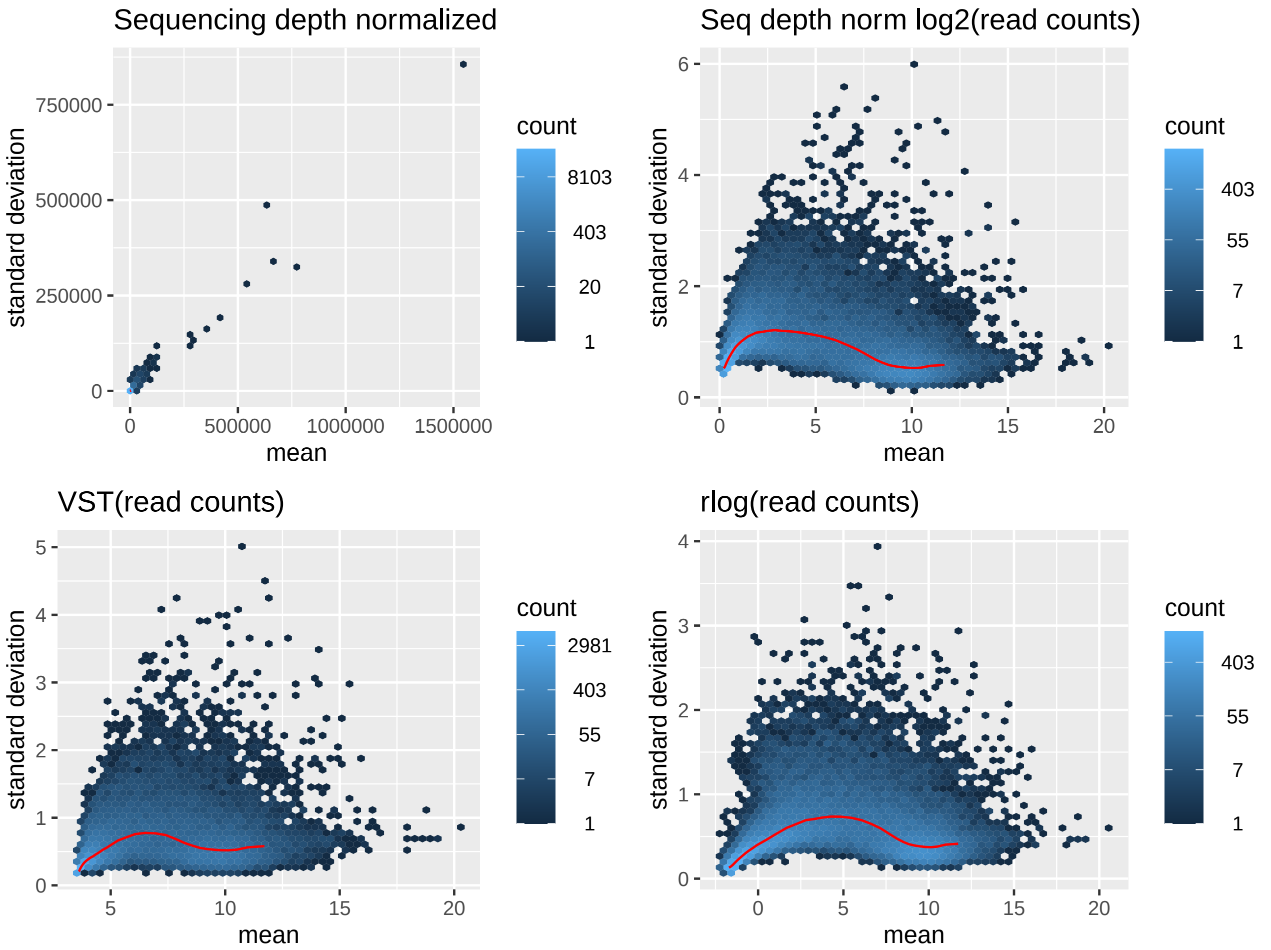

Figure B.2: Comparison of different normalization and data transformation methods for LOCRC samples. (a) Raw counts before normalization. (b) Normalized counts after sequencing depth normalization. (c) Normalized counts after variance stabilizing transformation (vst). (d) Normalized counts after regularized log transformation (rlog).

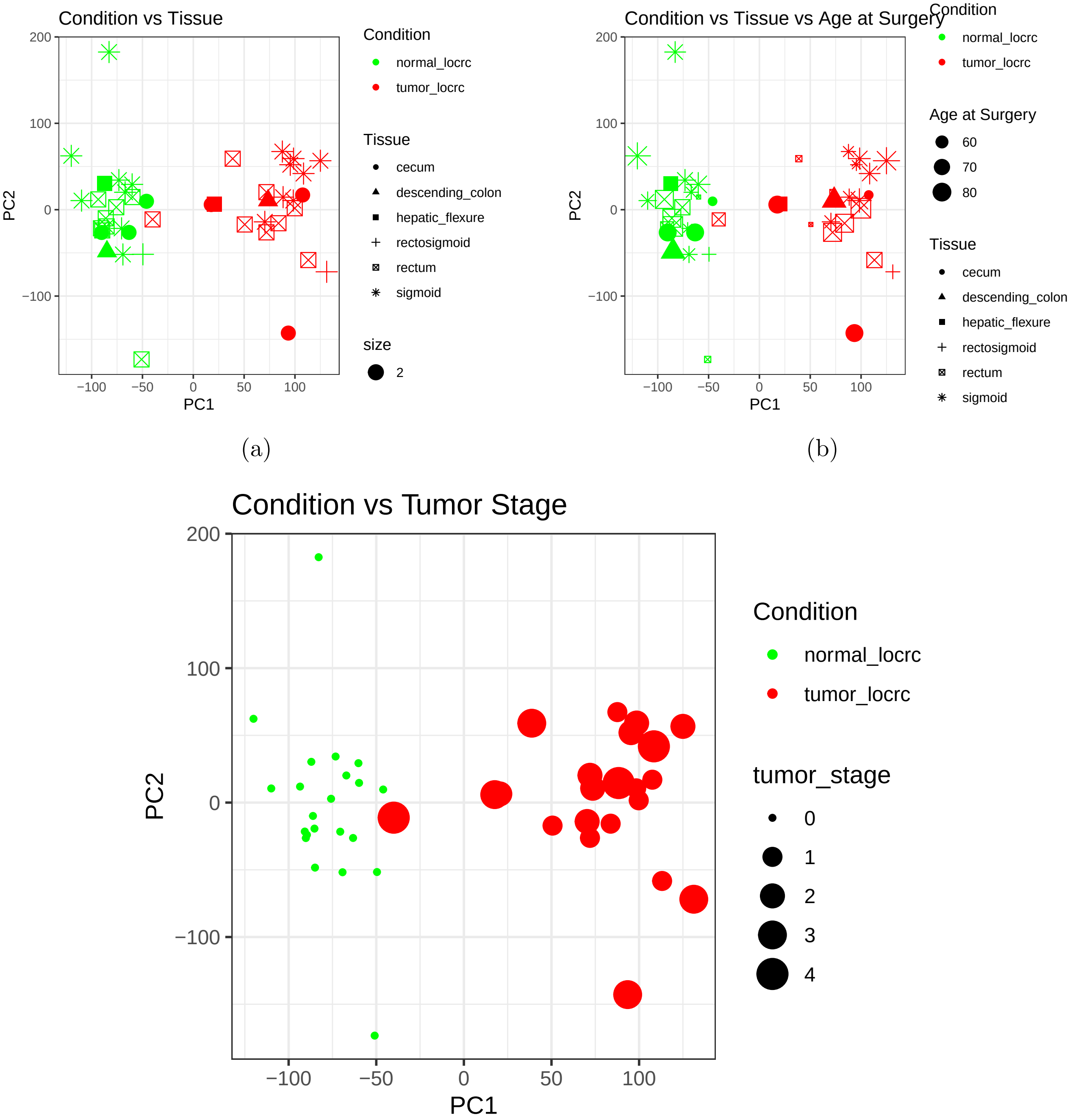

(a)

(b)

(c)

Figure B.3: PCA of LOCRC samples based on `condition & tissue`, `condition & tissue & age at surgery`, `condition & tumor stage`.

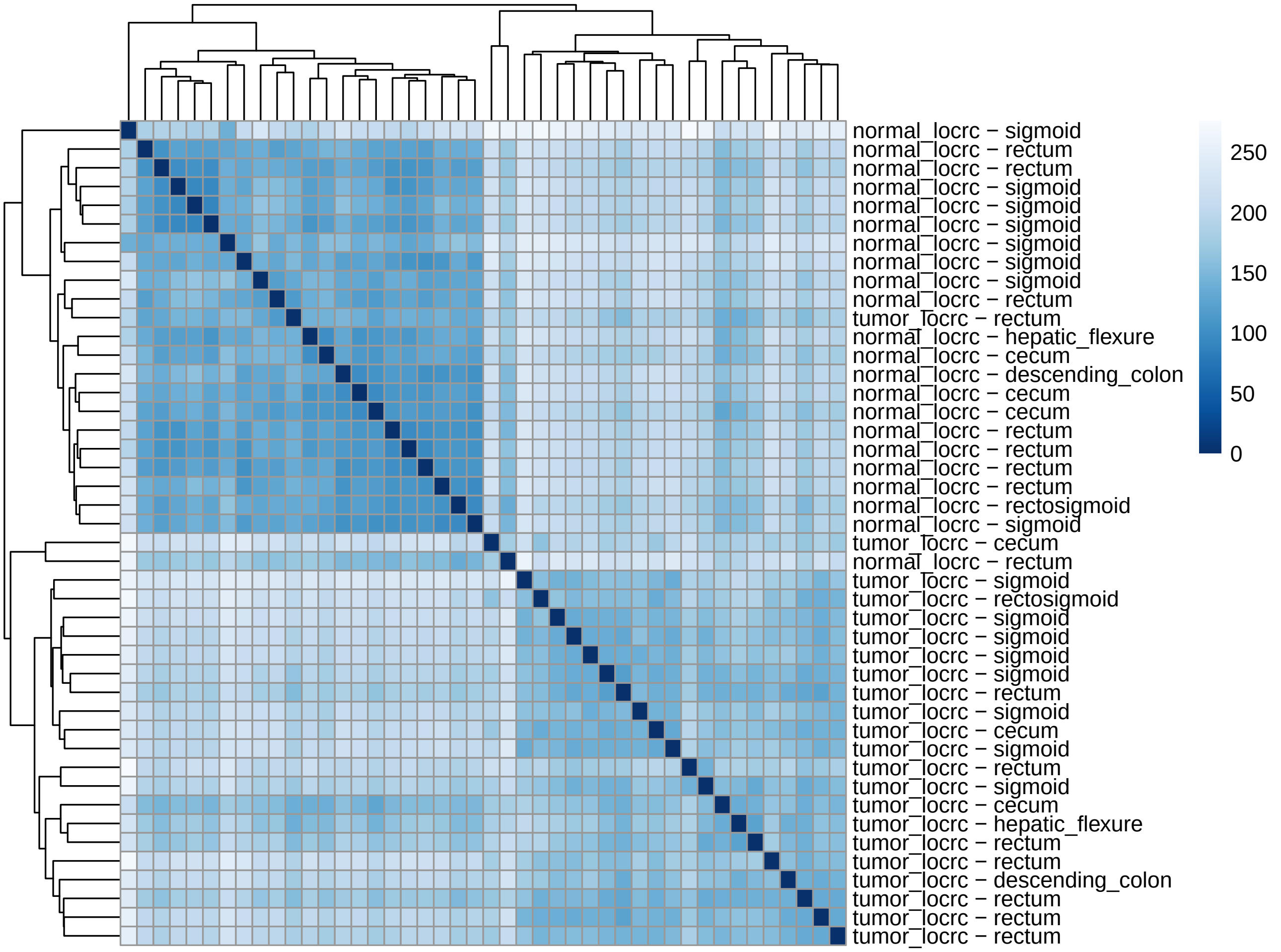

Figure B.4: Distance heatmap of LOCRC samples based on variance stabilizing transformation (vst) normalized counts. The heatmap displays hierarchical clustering of samples, with color intensity representing the distance between sample expression profiles.

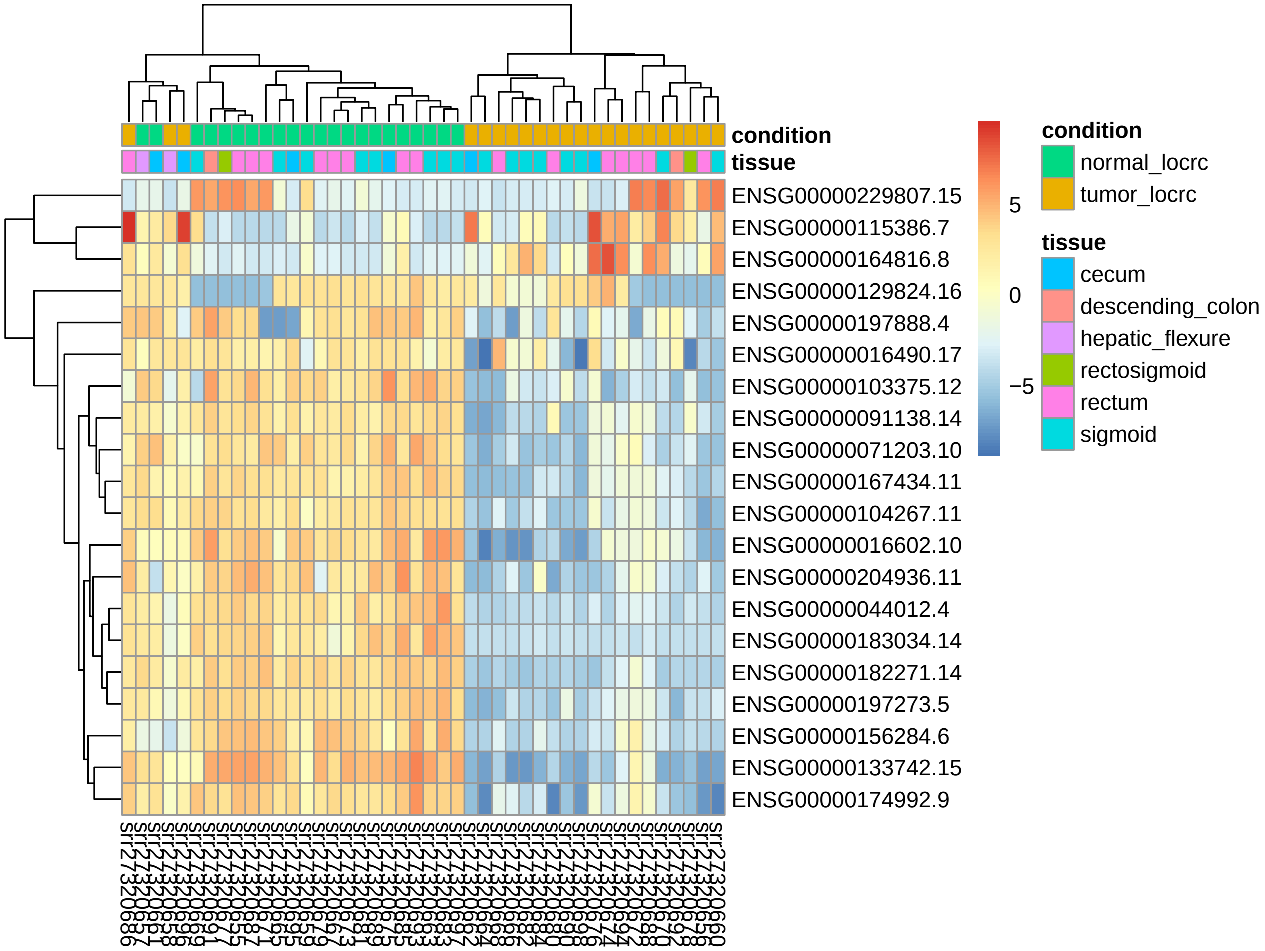

Figure B.5: Hierachical heatmap of LOCRC samples.

Table B.1: Top DEGs of the LOCRC cohort.

	Gene	baseMean	log2FoldChange	padj
ENSG00000175832	ETV4	777.7	5.908	6.42e-100
ENSG00000164379	FOXQ1	554.6	6.813	3.43e-68
ENSG00000173898	SPTBN2	335.2	3.844	1.42e-61
ENSG00000287828	NA	117.9	3.743	2.31e-55
ENSG00000111110	PPM1H	475.6	2.841	8.86e-53
ENSG00000165816	VWA2	447.5	4.612	4.59e-49
ENSG00000164283	ESM1	72.8	5.750	2.78e-48
ENSG00000015413	DPEP1	1834.3	6.596	1.12e-47
ENSG00000120708	TGFBI	8131.2	2.903	1.07e-46
ENSG00000162073	PAQR4	378.3	1.920	1.99e-45
ENSG00000214039	LINC02418	301.2	8.239	3.19e-45
ENSG00000186462	NAP1L2	52.1	-3.451	4.65e-45
ENSG00000183734	ASCL2	740.2	4.241	5.55e-45
ENSG00000172031	EPHX4	78.0	5.329	1.47e-43
ENSG00000163347	CLDN1	850.1	4.858	4.30e-43
ENSG00000165905	LARGE2	185.1	4.659	4.30e-43
ENSG00000128059	PPAT	488.3	2.212	1.28e-41
ENSG00000071539	TRIP13	299.5	2.990	2.43e-41
ENSG00000281406	BLACAT1	105.6	5.527	5.36e-40
ENSG00000171617	ENC1	2115.8	2.004	1.75e-39
ENSG00000219481	NBPF1	1163.8	-2.384	3.03e-39
ENSG00000103494	RPGRIP1L	191.4	2.022	6.73e-39
ENSG00000103888	CEMIP	1134.0	4.976	8.27e-39
ENSG00000165376	CLDN2	971.6	7.699	1.08e-38
ENSG00000120254	MTHFD1L	472.9	2.701	1.74e-38
ENSG00000169247	SH3TC2	174.7	3.959	2.01e-38
ENSG00000185269	NOTUM	222.7	8.730	2.83e-38
ENSG00000103021	CFAP263	136.9	2.115	3.03e-38
ENSG00000105948	IFT56	137.2	2.313	4.40e-38
ENSG00000123643	SLC36A1	1170.9	-2.367	6.16e-38

Appendix C

DTU analysis supplementary data

Table C.1: Top isoforms from each comparison `normal_eocrc vs tumor_eocrc and normal_locrc vs tumor_locrc` ordered by `q-value`.

Isoform ID	Gene ID	Condition 1	Condition 2	dIF	q-value	Rank
ENST00000378292.9	TPM2	normal_eocrc	tumor_eocrc	-0.133	0.0001117	1
ENST00000698539.1	SORBS2	normal_locrc	tumor_locrc	-0.233	0.0001545	2
ENST00000378292.9	TPM2	normal_locrc	tumor_locrc	-0.173	0.0001545	3
ENST00000642527.1	FSIP1	normal_locrc	tumor_locrc	0.112	0.0001622	4
ENST00000319481.8	OSBPL1A	normal_locrc	tumor_locrc	0.294	0.0002382	5
ENST00000338983.7	MAP3K20	normal_locrc	tumor_locrc	-0.273	0.0003502	6
ENST00000263398.11	CD44	normal_locrc	tumor_locrc	-0.311	0.0004923	7
ENST00000374429.6	CXCL12	normal_locrc	tumor_locrc	0.214	0.0006191	8
ENST00000865845.1	NLN	normal_locrc	tumor_locrc	0.203	0.0006191	9
ENST00000316673.9	HNF4A	normal_locrc	tumor_locrc	0.408	0.0009308	10
ENST00000637069.1	KIAA1671	normal_locrc	tumor_locrc	0.318	0.0016565	11
ENST00000356861.9	TNPO2	normal_locrc	tumor_locrc	-0.423	0.0016565	12
ENST00000885410.1	SESN1	normal_locrc	tumor_locrc	-0.150	0.0018008	13
ENST00000329305.6	TPM2	normal_locrc	tumor_locrc	0.115	0.0018008	14
ENST00000373827.6	ANK3	normal_locrc	tumor_locrc	0.139	0.0019256	15
ENST00000415602.5	TCEA2	normal_eocrc	tumor_eocrc	0.116	0.0020556	16
ENST00000433644.2	FANCC	normal_locrc	tumor_locrc	0.235	0.0020820	17
ENST00000507460.1	GABRA2	normal_locrc	tumor_locrc	0.133	0.0020820	18
ENST00000635823.2	KIF16B	normal_locrc	tumor_locrc	-0.305	0.0020820	19
ENST00000624247.1	SMTN	normal_locrc	tumor_locrc	-0.176	0.0022917	20
ENST00000489337.5	SMTN	normal_locrc	tumor_locrc	0.076	0.0024667	21
ENST00000329305.6	TPM2	normal_eocrc	tumor_eocrc	0.101	0.0025112	22
ENST00000532465.1	LMNB2	normal_locrc	tumor_locrc	-0.246	0.0029059	23
ENST00000325327.4	LMNB2	normal_locrc	tumor_locrc	0.232	0.0029544	24
ENST00000367514.7	C1orf21	normal_locrc	tumor_locrc	0.337	0.0030037	25
ENST00000454658.6	SINHCAF	normal_locrc	tumor_locrc	-0.101	0.0030037	26
ENST00000412051.5	CHLSN	normal_locrc	tumor_locrc	-0.269	0.0031328	27

Continued on next page

Table C.1 (continued from previous page)

Isoform ID	Gene ID	Condition 1	Condition 2	dIF	q-value	Rank
ENST00000393414.6	IL1R2	normal_locrc	tumor_locrc	0.248	0.0040455	28
ENST00000301843.13	CTTN	normal_locrc	tumor_locrc	0.235	0.0041748	29
ENST00000705474.1	TNS3	normal_locrc	tumor_locrc	-0.264	0.0041748	30
ENST00000361901.6	CALD1	normal_locrc	tumor_locrc	0.277	0.0045070	31
ENST00000316099.10	HNF4A	normal_locrc	tumor_locrc	-0.421	0.0045070	32
ENST00000337130.10	UGP2	normal_locrc	tumor_locrc	-0.436	0.0048100	33
ENST00000539026.1	LINC01559	normal_eocrc	tumor_eocrc	-0.160	0.0050706	34
ENST00000382040.4	RSAD2	normal_eocrc	tumor_eocrc	-0.157	0.0050706	35
ENST00000341723.8	HEPACAM2	normal_locrc	tumor_locrc	-0.255	0.0055968	36
ENST00000391839.6	COX20	normal_locrc	tumor_locrc	-0.167	0.0057885	37
ENST00000378943.7	GK	normal_locrc	tumor_locrc	0.231	0.0057931	38
ENST00000283365.14	DTNA	normal_locrc	tumor_locrc	0.100	0.0060797	39
ENST00000904832.1	ACTN1	normal_locrc	tumor_locrc	-0.171	0.0061631	40
ENST00000318426.6	LINC01559	normal_eocrc	tumor_eocrc	0.139	0.0062714	41
ENST00000871508.1	UGT2B15	normal_locrc	tumor_locrc	-0.536	0.0069021	42
ENST00000394468.7	HEPACAM2	normal_locrc	tumor_locrc	0.160	0.0071537	43
ENST00000399443.7	OSBPL1A	normal_locrc	tumor_locrc	-0.341	0.0071537	44
ENST00000222902.7	CCL24	normal_locrc	tumor_locrc	-0.280	0.0073466	45
ENST00000449201.5	NT5C3A	normal_locrc	tumor_locrc	-0.113	0.0073466	46
ENST00000610140.7	NT5C3A	normal_locrc	tumor_locrc	0.142	0.0078493	47
ENST00000864419.1	RERE	normal_locrc	tumor_locrc	0.146	0.0080275	48
ENST00000415691.2	HNF4A	normal_locrc	tumor_locrc	-0.056	0.0081462	49
ENST00000373672.8	COL16A1	normal_locrc	tumor_locrc	-0.204	0.0086799	50
ENST00000570103.5	CFDP1	normal_locrc	tumor_locrc	-0.324	0.0088678	51
ENST00000560234.1	PCLAF	normal_locrc	tumor_locrc	-0.193	0.0088678	52
ENST00000283882.4	CFDP1	normal_locrc	tumor_locrc	0.288	0.0088928	53
ENST00000394417.7	UGP2	normal_locrc	tumor_locrc	0.420	0.0093767	54
ENST00000406659.3	DNMT3A	normal_locrc	tumor_locrc	-0.127	0.0104062	55
ENST00000354655.9	ACSL5	normal_locrc	tumor_locrc	-0.282	0.0105226	56
ENST00000563608.2	PRMT7	normal_locrc	tumor_locrc	-0.204	0.0105784	57
ENST00000262820.7	KLHL13	normal_locrc	tumor_locrc	0.096	0.0109470	58
ENST00000380291.5	AP1S2	normal_locrc	tumor_locrc	0.089	0.0119636	59
ENST00000467155.7	HOXB-AS3	normal_locrc	tumor_locrc	-0.137	0.0119636	60
ENST00000630269.2	MLLT3	normal_locrc	tumor_locrc	0.189	0.0119636	61
ENST00000393353.7	FHL2	normal_locrc	tumor_locrc	0.116	0.0126306	62
ENST00000490982.1	TRPM2	normal_locrc	tumor_locrc	0.422	0.0126306	63
ENST00000216129.7	TTLL12	normal_locrc	tumor_locrc	0.337	0.0126306	64
ENST00000866634.1	UBXN10	normal_locrc	tumor_locrc	0.327	0.0126306	65
ENST00000305139.11	UGT1A6	normal_locrc	tumor_locrc	0.359	0.0136912	66
ENST00000416943.1	CCL24	normal_locrc	tumor_locrc	0.210	0.0141782	67
ENST00000859089.1	KHNYN	normal_locrc	tumor_locrc	-0.375	0.0141782	68
ENST00000697576.1	ZNF44	normal_locrc	tumor_locrc	0.121	0.0141782	69
ENST00000746568.1	SPEN-AS1	normal_locrc	tumor_locrc	0.376	0.0141972	70
ENST00000887088.1	TNS3	normal_locrc	tumor_locrc	0.063	0.0146668	71

Continued on next page

Table C.1 (continued from previous page)

Isoform ID	Gene ID	Condition 1	Condition 2	dIF	q-value	Rank
ENST00000297268.11	COL1A2	normal_eocrc	tumor_eocrc	0.193	0.0155919	72
ENST00000532465.1	LMNB2	normal_eocrc	tumor_eocrc	-0.190	0.0163917	73
ENST00000489749.1	RSAD2	normal_eocrc	tumor_eocrc	0.117	0.0163917	74
ENST00000601295.2	ZNF708	normal_locrc	tumor_locrc	0.272	0.0182954	75
ENST00000397317.8	CLDN7	normal_locrc	tumor_locrc	-0.158	0.0185549	76
ENST00000458715.5	COL16A1	normal_locrc	tumor_locrc	-0.064	0.0188584	77
ENST00000307486.12	MAB21L4	normal_locrc	tumor_locrc	-0.485	0.0190188	78
ENST00000737891.1	ENSG00000296299	normal_locrc	tumor_locrc	-0.229	0.0201571	79
ENST00000322142.13	FHL2	normal_locrc	tumor_locrc	-0.102	0.0204909	80
ENST00000369856.8	FLNA	normal_locrc	tumor_locrc	0.147	0.0207518	81
ENST00000355288.6	ANK3	normal_locrc	tumor_locrc	-0.206	0.0207739	82
ENST00000955652.1	FAM200A	normal_locrc	tumor_locrc	-0.347	0.0210044	83
ENST00000851604.1	SLC39A14	normal_locrc	tumor_locrc	0.175	0.0211065	84
ENST00000913175.1	VSNL1	normal_locrc	tumor_locrc	-0.100	0.0212544	85
ENST00000509819.1	ABLIM2	normal_locrc	tumor_locrc	-0.323	0.0217980	86
ENST00000515595.1	NLN	normal_locrc	tumor_locrc	-0.366	0.0217980	87
ENST00000526995.6	TRAF6	normal_locrc	tumor_locrc	0.228	0.0217980	88
ENST00000325327.4	LMNB2	normal_eocrc	tumor_eocrc	0.192	0.0220051	89
ENST00000338983.7	MAP3K20	normal_eocrc	tumor_eocrc	-0.217	0.0220051	90
ENST00000875353.1	PPARD	normal_locrc	tumor_locrc	-0.419	0.0225768	91
ENST00000439587.6	TMEM8B	normal_locrc	tumor_locrc	0.233	0.0230987	92
ENST00000899612.1	RAB27A	normal_locrc	tumor_locrc	-0.271	0.0239662	93
ENST00000559547.1	FSIP1	normal_locrc	tumor_locrc	-0.611	0.0242630	94
ENST00000247829.8	TSPAN8	normal_locrc	tumor_locrc	0.230	0.0243448	95
ENST00000408042.5	KIF16B	normal_locrc	tumor_locrc	-0.101	0.0251548	96
ENST00000851603.1	SLC39A14	normal_locrc	tumor_locrc	-0.263	0.0260724	97
ENST00000290079.9	TMEM141	normal_locrc	tumor_locrc	-0.138	0.0261822	98
ENST00000428004.6	ABLIM2	normal_locrc	tumor_locrc	0.167	0.0281337	99
ENST00000301420.3	KLK1	normal_locrc	tumor_locrc	-0.224	0.0285900	100
ENST00000450644.2	AP1S2	normal_locrc	tumor_locrc	0.103	0.0293481	101
ENST00000590247.7	PDCD5	normal_locrc	tumor_locrc	-0.173	0.0298075	102
ENST00000606752.1	USP6NL	normal_locrc	tumor_locrc	-0.126	0.0298075	103
ENST00000933817.1	NVL	normal_locrc	tumor_locrc	-0.345	0.0303730	104
ENST00000371878.5	KLHL13	normal_locrc	tumor_locrc	0.109	0.0310361	105
ENST00000699484.1	CLCA4-AS1	normal_locrc	tumor_locrc	0.179	0.0311711	106
ENST00000676000.1	PURA	normal_locrc	tumor_locrc	0.197	0.0311711	107
ENST00000356644.7	SESN1	normal_locrc	tumor_locrc	0.135	0.0311711	108
ENST00000360325.11	CLDN7	normal_locrc	tumor_locrc	0.156	0.0317246	109
ENST00000892260.1	EIF4EBP2	normal_locrc	tumor_locrc	-0.106	0.0319195	110
ENST00000493364.1	HM13	normal_locrc	tumor_locrc	-0.141	0.0323757	111
ENST00000449309.2	FAM200A	normal_locrc	tumor_locrc	0.311	0.0328119	112
ENST00000596300.1	KLK1	normal_locrc	tumor_locrc	0.205	0.0328119	113
ENST00000361198.9	LDB1	normal_locrc	tumor_locrc	0.102	0.0328119	114
ENST00000705192.1	TNC	normal_locrc	tumor_locrc	0.103	0.0328119	115

Continued on next page

Table C.1 (continued from previous page)

Isoform ID	Gene ID	Condition 1	Condition 2	dIF	q-value	Rank
ENST00000397928.6	TRPM2	normal_locrc	tumor_locrc	-0.504	0.0328119	116
ENST00000392359.8	CENPX	normal_locrc	tumor_locrc	-0.152	0.0330643	117
ENST00000373218.5	EIF4EBP2	normal_locrc	tumor_locrc	0.106	0.0330643	118
ENST00000851597.1	SLC39A14	normal_locrc	tumor_locrc	-0.066	0.0341478	119
ENST00000477428.5	NRF1	normal_locrc	tumor_locrc	0.144	0.0348101	120
ENST00000494035.1	TTLL12	normal_locrc	tumor_locrc	-0.263	0.0351177	121
ENST00000586035.1	PDCD5	normal_locrc	tumor_locrc	0.159	0.0359078	122
ENST00000377351.8	UBA1	normal_locrc	tumor_locrc	0.198	0.0361055	123
ENST00000256078.10	KRAS	normal_locrc	tumor_locrc	-0.212	0.0362730	124
ENST00000433510.3	LINC03057	normal_locrc	tumor_locrc	-0.198	0.0366792	125
ENST00000465485.1	FRMD3	normal_locrc	tumor_locrc	0.108	0.0370495	126
ENST00000409569.3	MIR4435-2HG	normal_locrc	tumor_locrc	0.469	0.0378273	127
ENST00000467155.7	HOXB-AS3	normal_eocrc	tumor_eocrc	-0.107	0.0379573	128
ENST00000464702.6	PDPK1	normal_locrc	tumor_locrc	0.168	0.0399077	129
ENST00000380321.5	MLLT3	normal_locrc	tumor_locrc	-0.180	0.0412451	130
ENST00000481284.5	ACSS2	normal_locrc	tumor_locrc	-0.231	0.0423638	131
ENST00000477565.3	BORCS8	normal_locrc	tumor_locrc	0.164	0.0427973	132
ENST00000566543.1	PDP2	normal_locrc	tumor_locrc	-0.101	0.0428721	133
ENST00000370671.7	SAMD13	normal_locrc	tumor_locrc	-0.156	0.0431237	134
ENST00000484879.1	RB1	normal_locrc	tumor_locrc	-0.121	0.0442143	135
ENST00000244709.9	TREM1	normal_locrc	tumor_locrc	-0.138	0.0443872	136
ENST00000555292.1	ABHD12B	normal_locrc	tumor_locrc	-0.149	0.0450080	137
ENST00000721369.1	ENSG00000294133	normal_locrc	tumor_locrc	-0.377	0.0450080	138
ENST00000483187.5	TMEM141	normal_locrc	tumor_locrc	0.124	0.0450385	139
ENST00000419155.5	PHF19	normal_locrc	tumor_locrc	-0.159	0.0450547	140
ENST00000774911.1	HSD11B1-AS1	normal_eocrc	tumor_eocrc	0.259	0.0450650	141
ENST00000355841.7	PDLIM7	normal_eocrc	tumor_eocrc	0.141	0.0450650	142
ENST00000608940.2	LINC03057	normal_locrc	tumor_locrc	0.178	0.0453906	143
ENST00000339413.11	YIF1B	normal_locrc	tumor_locrc	-0.189	0.0453906	144
ENST00000565575.1	CLCA4-AS1	normal_locrc	tumor_locrc	-0.186	0.0468901	145
ENST00000374426.6	CXCL12	normal_locrc	tumor_locrc	0.091	0.0468901	146
ENST00000465125.2	RERE	normal_locrc	tumor_locrc	-0.190	0.0468901	147
ENST00000931078.1	ENAH	normal_locrc	tumor_locrc	-0.203	0.0485547	148

Appendix D

RNA secondary prediction analysis supplementary data

Listing D.1: FASTA sequences of the top 10 isoforms exhibiting differential transcript usage (DTU) in EOCRC.

```
>ENST00000378292.9
GCGGCCGCACCCCCCGGCCGGGCCGTGCTTCTGCCCCTACAAGGTTTGGGCCGAGGTGGGGGAGGGTCCTGGTTGCCGGC

>ENST00000415602.5
GGCAGGACGAGACCCCTCCCCGGCAGAGACTAACCGGGACGCAGGGGAGACCCCCACCCGTGGCCGAGACCCCTGCCCCG

>ENST00000329305.6
TCCTCCTCGCCTGCCACCGGTGCACCCAGTCCGCTCACCCAGCCCAGTCCGTCCGGTCCTCACCGCCTGCCGGCCGGCCC

>ENST00000539026.1
AAATTTGTTGGCTGCTTGAGCTGGGATATTCATCTTTCTCCTGATCTTGGACATCAGAACTCCTGATTCTCAAGCCTTTG

>ENST00000382040.4
GCTCTGCTCCAGGCATCTGCCACAATGTGGGTGCTTACACCTGCTGCTTTTGCTGGGAAGCTCTTGAGTGTGTTCAGGCA

>ENST00000318426.6
GCAGACTTGAATAGAACTAAAAGGAAGAGGAAGGGCAAATTTGTTGGCTGCTTGAGCTGGGATATTCATCTTTCTCCTGA

>ENST00000297268.11
AGCACCACGGCAGCAGGAGGTTTCGGCTAAGTTGGAGGTACTGGCCACGACTGCATGCCCGCGCCCGCCAGGTGATACCT

>ENST00000532465.1
CCTCGGGTAGCGTCAGCATCGAGGAGATCGACCTGGAGGGCAAGTTTGTGCAGCTCAAGAACAACTCGGACAAGGATCAG

>ENST00000489749.1
GTCAACTATCACTTCACTCGCCAGTGCAACTACAAATGCGGCTTCTGTTTCCACACAGCCAAAACATCCTTTGTGCTGCC

>ENST00000325327.4
ATCTTGCAGCCGGCGGCGCGGATTGAATGAGCCCGCCGAGCCCGGGCCGCCGTCGGGAGCAGCGCAGGCCGCGAGCCGCC
```

Listing D.2: FASTA sequences of the top 10 isoforms exhibiting differential transcript usage (DTU) in LOCRC.

```
>ENST00000698539.1
AGCAGTAGCAGAGGCAGCTTCTGAGAGCCTGGGCAGGCAGCAGCTGGCTGACCAAGTCCACTGGAAGAGAAGGCTTGTGC

>ENST00000378292.9
GCGGCCGCACCCCCCGGCCGGGCCGTGCTTCTGCCCCTACAAGGTTTGGGCCGAGGTGGGGGAGGGTCCTGGTTGCCGGC

>ENST00000642527.1
AGAGTCCACATCATGTCTCTCTGAAGAACAGTTAAAGTGTCTTCTGGATGAATGCATACTTAAACAAAAATCCATCATTA

>ENST00000319481.8
GTGGTCCCGGCGCCGGGTCCCGGAGACAGACGTTACGCGGGCTCGAGCGTCCTCGGGGAGTGCCAGCCAGAGTTGGTGAC

>ENST00000338983.7
CTTCCTCATTGGCGCCGTGCAGAGAGGCGGAATGTTCAACTCCTAACTGCAGCGGAAACGTGGGAGCCGCGCGGGCCGCT

>ENST00000263398.11
CTCATTGCCCAGCGGACCCCAGCCTCTGCCAGGTTCGGTCCGCCATCCTCGTCCCGTCCTCCGCCGGCCCCTGCCCCGCG

>ENST00000374429.6
ACTTTCACTCTCCGTCAGCCGCATTGCCCGCTCGGCGTCCGGCCCCCGACCCGCGCTCGTCCGCCCGCCCGCCCGCCCGC

>ENST00000865845.1
AGGCAGCCACTGTGGCCTCTGCGGCTAGGCCGGCTCGAGACTCCCGGGCGCCCAGGCGCTGCCGCCCGCCTCGCCGCCCC

>ENST00000316673.9
GCACTCACCGCCTTCCTGGTGGACGGGCTCCTGGTGGCTGTGCTGCTGCTGTGAGCGGGCCCCTGCTCCTCCATGCCCCC

>ENST00000637069.1
CTCCTTGTCTCGGCCGATCAGCTGGGTGAGCCCTGGAACTGGAACCTGGACTGCCCAGTGTGTTGACTTTATAACTCCGC
```